This is the peer-reviewed, final accepted version for American Mineralogist, published by the Mineralogical Society of America.
The published version is subject to change. Cite as Authors (Year) Title. American Mineralogist, in press.
DOI: https://doi.org/10.2138/am-2022-8211. http://www.minsocam.org/

Revision 2

A COMPARATIVE STUDY OF TWO PHASE EQUILIBRIA MODELING TOOLS: MORB EQUILIBRIUM STATES AT VARIABLE PRESSURE AND H_2O CONCENTRATIONS

Word count: 9504

David Hernández-Uribe[1*], Frank J. Spera[2], Wendy A. Bohrson[3], Jussi S. Heinonen[4]

[1]*Department of Earth and Environmental Sciences, University of Michigan, MI, USA*

[2]*Department of Earth Science and Earth Research Institute, University of California, Santa Barbara, CA, USA*

[3]*Department of Geology and Geological Engineering, Colorado School of Mines, CO, USA*

[4]*Department of Geosciences and Geography, University of Helsinki, Helsinki, Finland*

*corresponding author: dav.hernandez.uribe@gmail.com

ABSTRACT

Phase equilibria modeling is a powerful petrological tool to address both forward and inverse geological problems over a broad range of crustal and upper mantle conditions of pressure (P), temperature (T), composition (X) and redox (f_{O2}). The development of thermodynamic databases, relatively realistic activity–composition (a–X) relations for solids, melts and fluids, pressure-volume-temperature (PVT) equations of state (EOS), and efficient numerical algorithms

Always consult and cite the final, published document. See http:/www.minsocam.org or GeoscienceWorld

This is the peer-reviewed, final accepted version for American Mineralogist, published by the Mineralogical Society of America.
The published version is subject to change. Cite as Authors (Year) Title. American Mineralogist, in press.
DOI: https://doi.org/10.2138/am-2022-8211. http://www.minsocam.org/

represent an inflection point in our ability to understand the nexus between tectonics and petrogenesis. While developed—and typically applied in isolation—by either metamorphic or igneous petrologists, some of the published thermodynamic models have overlapping *P–T–X* calibration ranges, which enables comparisons of model outcomes for similar conditions within the range of applicability. In this paper, we systematically compare the results of two such models that are routinely used for calculating phase equilibria in melt-bearing systems: rhyolite-MELTS (Ghiorso et al., 2012; Ghiorso and Gualda, 2015) and the metabasite set of Green et al. (2016) using the thermodynamic database ds62 (Holland and Powell, 2011) (hereafter denoted as "HPx-mb16"). We selected a N-MORB composition and modeled closed system equilibrium phase relations as a function of temperature at 0.25 GPa and 1 GPa for N-MORB with 0.5 wt% and 4 wt% H_2O. Our results show that phase relations exhibit some key differences that, in some instances, impact geological inferences. For example, clinopyroxene and plagioclase stabilities are expanded to higher temperatures in HPx-mb16 compared to predictions from rhyolite-MELTS. Orthopyroxene and olivine are stable in greater proportions and at wider temperature ranges in rhyolite-MELTS compared to HPx-mb16. Importantly, HPx-mb16 predicts amphibole in all runs presented here, whereas amphibole is only predicted at high-*P*–high-H_2O (1 GPa and 4 wt% H_2O) in rhyolite-MELTS, and in lesser amounts. Garnet stability is systematically expanded at higher temperatures and the proportion is greater in rhyolite-MELTS. In addition to phase assemblage differences, phase compositions may differ. For example, plagioclase anorthite content is systematically higher in HPx-mb16 (for the same set of conditions) whereas garnet Mg# is higher in rhyolite-MELTS. Calculated amphibole compositions are substantially different between the two models as well. Liquid compositions also show important differences. High-*T* liquids are generally similar in SiO_2 contents but diverge at lower temperatures; in these cases,

Always consult and cite the final, published document. See http:/www.minsocam.org or GeoscienceWorld

HPx-mb16 liquids are SiO_2-depleted compared to those produced by rhyolite-MELTS. Liquids are also systematically and substantially more mafic in HPx-mb16, and alumina and the alkali concentrations are relatively different and show different trends as a function of temperature at constant pressure. Overall, liquid compositions show the greatest differences near the solidus. Differences in modal abundances of phases and liquid compositions influence liquid trace-element signatures, and these differences can affect geological interpretations. Finally, a comparison between melting experiments of basaltic bulk composition and both thermodynamic models shows that rhyolite-MELTS better reproduces the higher temperature experiments, whereas HPx-mb16 better reproduces the lower temperature experiments. We discuss these and other similarities and differences in order to highlight the strengths and limitations of each model, and to recognize that modeling results have important implications for interpretations of geologic processes. We recognize that our results are informed by a small subset of calculations over a limited range of conditions—our results encourage further comparisons over a wider range of conditions and compositions.

Key words: phase equilibria modeling, computational petrology, rhyolite-MELTS, Theriak-Domino, thermodynamics

INTRODUCTION

The use of thermodynamics to comprehensively model multiphase and multicomponent igneous and metamorphic systems is one of the most important developments in the Earth Sciences of the past several decades (Ghiorso and Sack, 1995; Powell et al., 1998). Phase equilibria modeling can predict equilibrium phase relationships over a wide range of pressure and temperature conditions (*P–T*) for a

Always consult and cite the final, published document. See http:/www.minsocam.org or GeoscienceWorld

variety of bulk compositions at various redox conditions (Powell et al., 1998, 2005; Powell and Holland, 2008; Gaulda et al., 2012). While there are inherent limitations associated with the use of any phase equilibrium model—including the neglect of reaction kinetics, solid and liquid state diffusion, spatial *P*–*T* gradients, and uncertainties associated with thermodynamic properties of relevant substances—their utility to reproduce first-order observations of key Earth processes is evident (see, e.g., seminal work of Bowen, 1928, 1945; Thompson, 1967; Carmichael et al., 1974). Successes include phase equilibria modeling that has described magmatic systems and metamorphism in a host of environments including volcanic arcs, subduction zones, orogenic terranes, and large igneous provinces (e.g. Kerrick and Connolly, 2001; White and Powell, 2002; Johnson et al., 2008; Fowler and Spera, 2010; Bohrson et al., 2014; Yakymchuck and Brown, 2014; García-Arias and Stevens, 2017; Palin et al., 2017; Hernández-Uribe and Palin, 2019; Heinonen et al., 2019; among many others).

Crystallization and partial melting are crucial for understanding heat advection and matter exchange between the mantle and the crust as the formation, extraction, ascent and crystallization of magma is a primary mechanism that leads to differentiation on Earth and other planerary bodies (England and Thompson, 1986; Brown, 2007). Accurate phase equilibria predictions (of liquid-bearing systems) are thus key components of the earth scientist's toolbox to understand crucial geological processes. Multiphase and multicomponent thermodynamic modeling of partially or totally molten systems has been possible since the 1980's and the pioneering efforts have been greatly extended and improved over the past thirty years (Berman, 1988; Essene, 1989; Holland and Powell, 1998, 2011; Ghiorso and Sack, 1995; Ghiorso, 2004). Standard state thermodynamic data, volatile species pressure-volume-temperature (*PVT*) data, and activity–composition (*a*–*X*) relations for crystalline and liquid solutions (collectively referred hereafter as " the thermodynamic model") commonly used in igneous petrology include those in the MELTS package (rhyolite-MELTS, pMELTS, and pHMELTS

Always consult and cite the final, published document. See http:/www.minsocam.org or GeoscienceWorld

calibrations; Ghiorso and Sack, 1995; Asimow and Ghiorso, 1998; Ghiorso et al., 2002; Asimow et al., 2004; Gualda et al., 2012; Ghiorso and Gualda, 2015). The thermodynamic model commonly used in metamorphic petrology is mostly based on the work of Powell and Holland (1988) and Holland and Powell (1998, 2011), although there are other examples (cf., Lanari and Duesterhoeft, 2018). For metamorphic systems, modeling of granitic liquid compositions is possible with the White et al. (2014) silicate liquid *a–X* relations based on previous liquid relations (Holland and Powell, 1998, 2001; White et al., 2001, 2007), whereas basaltic melting can be modeled with the *a–X* relations of Jennings and Holland (2015) and Green et al. (2016). Updated *a–X* relations that allow modeling of melt-bearing equilibria in ultramafic-to-felsic metamorphic systems were recently published by Holland et al. (2018) and Tomlinson and Holland (2021). We emphasize that although different thermodynamic models are preferred by igneous and metamorphic petrologists, the models have overlapping calibration ranges and are used for exactly the same purpose—modeling phase equilibria and compositions in liquid-bearing silicate systems. At equilibrium closed-system conditions, partial melting of a metabasic lithology and crystallization of a basaltic liquid exhibit identical phase relations at a given *P–T* state point.

Despite the common use of phase equilibria modeling in petrology, to the best of our knowledge, there have not been systematic studies to examine differences among thermodynamic models where calibrations overlap. While the study of Jennings and Holland (2015) and Holland et al. (2018) do compare their *a–X* relations to results from pMELTS, the focus of those papers was not a systematic comparison of the predicted equilibria. Existing comparative studies in metamorphic petrology explore the differences of the various Holland and Powell thermodynamic databases (e.g. Korhonen et al., 2014; Guevara and Caddick, 2016; Pan et al., 2020; Starr et al., 2020), and compare model predictions with experiments and natural samples (e.g. White et al., 2011; Forshaw et al., 2019; Santos et al., 2019; García-Arias, 2020;

Always consult and cite the final, published document. See http:/www.minsocam.org or GeoscienceWorld

Bartoli and Carvalho, 2021; Gervais and Trapy, 2021). The MELTS package collection has also been compared to results of other thermobarometic methods on natural samples (e.g., Pamukcu et al., 2015), experimental studies not included in the model calibrations (e.g., Hirschmann et al., 1998; Neave et al., 2019; Pichavant et al., 2019), and between different MELTS calibrations (e.g., Balta and McSween, 2013).

In this study, we take a combined approach. We systematically compare phase equilibria calcualted with rhyolite-MELTS (Ghiorso et al., 2012; Ghiorso and Gualda, 2015) and the "metabasite set" of Green et al. (2016) ("HPx-mb16", calculated using Theriak-Domino; de Capitani and Brown, 1987; de Capitani and Petrakakis, 2010) for the equilibrium states of a mid-ocean ridge basalt (MORB) at different *P–T* conditions and different initial H_2O contents from near-liquidus to solidus temperatures along the fayalite–magnetite–quartz (FMQ) oxygen buffer. These two thermodynamic approaches (i.e., rhyolite MELTS and HPx-mb16) are the most commonly used by igneous and metamorphic petrologists, respectively, to describe liquid-bearing mafic systems. We also evaluate how closely the calculated MORB phase equilibria between rhyolite-MELTS and HPx-mb16 compare with independent relevant experiments (i.e., not used in the calibration). We discuss the implications of our results within the framework of trace-element modeling and examine the geologic implications of the differences in model outcomes. By comparing the effects of pressure and H_2O concentration on the phase equilibria during equilibrium melting and crystallization of a MORB using two extant thermodynamic models, we provide our perspective on model uncertainty associated with the choice of modeling. The critical insight of our work is to recognize the strengths of the thermodynamic models, to highlight similarities and differences in order to illustrate how the choice of thermodynamic models can lead to different geologic interpretations.

Always consult and cite the final, published document. See http:/www.minsocam.org or GeoscienceWorld

This is the peer-reviewed, final accepted version for American Mineralogist, published by the Mineralogical Society of America.
The published version is subject to change. Cite as Authors (Year) Title. American Mineralogist, in press.
DOI: https://doi.org/10.2138/am-2022-8211. http://www.minsocam.org/

THERMODYNAMIC MODELS

Phase equilibria modeling relies on standard state thermodynamic data, EOS's and *a–X* relations for solid and liquid solutions. A thermodynamic database includes standard state properties for all phases, the form and numerical values defining *PVT*, and isobaric heat capacity expressions for all phases (Berman, 1988; Essene, 1989; Holland and Powell, 1998, 2011; Ghiorso and Sack, 1995; Ghiorso, 2004). These parameters are obtained from experimental, calorimetric and other studies (e.g., spectroscopy), and some are statistically treated to obtain the best-fit value for a desired parameter from multiple experiments (e.g., least-squares regressions used by Holland and Powell databases). In order to be "internally consistent", all thermodynamic parameters must be compatible with thermodynamic definitions and identities, adhere to a set of reference values, consider simultaneously all the experimental data, and reproduce primary data within their uncertainties (Lanari and Duesterhoeft, 2018, and references therein). The rhyolite-MELTS thermodynamic database is based on Berman (1988) with modifications (see Ghiorso and Sack, 1995; Asimow and Ghiorso, 1998; Gualda et al., 2012; Ghiorso and Gualda, 2015 for details). The thermodynamic data used in HPx-mb16 utilizes version 6.2 of Holland and Powell (2011). Some important differences between these thermodynamic data include—but are not limited to—how the equations of state of the solid phases are calculated (i.e. using the Tait equation of state in Holland and Powell (2011) vs. the EOS modified from Berman (1988) in the MELTS package) and the isobaric 1-bar heat capacity dependance on temperature (i.e., the Robie et al. (1978) equation in Holland and Powell (2011) vs. the high-*T* form used in the Berman and Brown (1985) equation for the MELTS package). Furthermore, the *PVT* properties of fluid utilized in the MELTS package are calculated using the model of Ghiorso and Gualda (2015),

Always consult and cite the final, published document. See http:/www.minsocam.org or GeoscienceWorld

whereas in Holland and Powell (2011) the equation of state of Pitzer and Sterner (1995) is used. For a comprehensive review of all the parameters used in these two thermodynamic models, the reader is referred to the original references.

In addition to standard state thermodynamic properties for pure phases, one must also treat the non-ideal properties of crystalline, liquid amd gaseous solutions. The excess Gibbs energies of multicomponent solutions are handled using *a–X* relations that relate Gibbs excess energies as a function of pressure, temperature, and solution composition to activity coefficients. The solid solution models describe the thermodynamics of mixing between end-members of the muticomponent solution and reflect the elemental substitutions that take place in crystalline solids including ordering and exsolution. The *a–X* relations for solid-solution phases commonly contain end-member proportions, crystallographic site fractions, mixing parameters (also known as the Margules parameter), ideal parameters, and thermodynamic adjustments (Lanari and Duesterhoeft, 2018, and references therein). Mixing relationships can be ideal, symmetrical, or asymmetrical, depending on the behavior of the Margules parameter pair. The excess Gibbs energy is normally a function of temperature and pressure. We discuss the *a–X* relations (and the elements considered) that were used in this work in the next section and other details are given in the Supplementary Table S1.

One approach to calculate phase equilibria is by solving simultaneous non-linear equations to build up an array of points and lines that make up the phase diagram by using Schreinemakers' analysis (e.g., THERMOCALC; Powell et al*.,* 1998), whereas another approach is Gibbs free energy minimization to determine the most stable phase assemblage at specific state points. This second approach is used in the MELTS package (Ghiorso and Sack, 1995; Asimow

Always consult and cite the final, published document. See http:/www.minsocam.org or GeoscienceWorld

This is the peer-reviewed, final accepted version for American Mineralogist, published by the Mineralogical Society of America.
The published version is subject to change. Cite as Authors (Year) Title. American Mineralogist, in press.
DOI: https://doi.org/10.2138/am-2022-8211. http://www.minsocam.org/

and Ghiorso, 1998; Gualda et al., 2012; Ghiorso and Gualda, 2015) and in Theriak-Domino and Perple_X (Connolly, 2005; de Capitani and Petrakakis, 2010).

PETROLOGICAL MODELING

Modeling setups

Phase equilibria calculations for this study were performed using rhyolite-MELTS and Theriak-Domino in the Na_2O–CaO–K_2O–FeO–MgO–Al_2O_3–SiO_2–H_2O–TiO_2–O_2 (NCKFMASHTO) system. This system was chosen because the HPx-mb16 model was calibrated in this 10-component system (Green et al., 2016), which is also appropriate for rhyolite-MELTS.

For the rhyolite-MELTS runs, we used the internally consistent thermodynamic database of Berman (1988) with some modifications (Gualda et al., 2012; Ghiorso and Gualda, 2015) and the *a–X* relations for solid-solution phases included in the rhyolite-MELTS calibration (Supplementary Table S1), i.e., silicate liquid (Ghiorso and Sack, 1995); pyroxene (Sack and Ghiorso, 1994); orthopyroxene, biotite, olivine (Sack and Ghiorso, 1989); amphibole (Ghiorso et al., 1995); garnet (Berman, 1990; Berman and Koziol, 1991); feldspar (Elkins and Grove,1990); spinel (Sack and Ghiorso 1991a, b); and rhombohedral oxide (Ghiorso, 1990; Ghiorso and Sack, 1991; Ghiorso and Evans, 2008). Note that, despite its name, rhyolite-MELTS is meant for modeling mafic systems and the prefix "rhyolite" only refers to the latest calibration that is more suitable also for felsic systems than the preceding MELTS versions (Gualda et al., 2012; http://melts.ofm-research.org).

For the Theriak-Domino runs, we utilized the Theriak-Domino version from D. K. Tinkham (https://dtinkham.net/peq.html), the internally consistent thermodynamic database ds62 (Holland and Powell, 2011), and the "metabasite set" of *a–X* relations for solution phases

Always consult and cite the final, published document. See http:/www.minsocam.org or GeoscienceWorld

This is the peer-reviewed, final accepted version for American Mineralogist, published by the Mineralogical Society of America.
The published version is subject to change. Cite as Authors (Year) Title. American Mineralogist, in press.
DOI: https://doi.org/10.2138/am-2022-8211. http://www.minsocam.org/

(Supplementary Table S1) from Green et al. (2016); these include: liquid, augite and clinoamphibole (Green et al., 2016); garnet, biotite, chloritoid, muscovite–paragonite, and chlorite (White et al., 2014); epidote (Holland and Powell, 2011); plagioclase (Holland and Powell, 2003); magnetite–spinel (White et al., 2002); and ilmenite–hematite (White et al., 2000). Pure phases include albite, quartz, rutile, and titanite.

In all comparative calculations in this study, we computed equilibrium state points only; fractionation was not used except as a preliminary step in rhyolite-MELTS to determine the appropriate version of rhyolite-MELTS. Hence our calculations apply equally to equilibrium crystallization and equilibrium partial melting as these processes are thermodynamically identical.

The wide *P*–*T*–*X* ranges of the modeling software enable near-infinite possibilities for model comparison. Here, we focus on a detailed comparison of one of the most widely used average compositions in petrological modeling, that of the mean N-MORB from Gale et al. (2013) (Table 1). Modeling intermediate and/or felsic systems is outside of the scope of this study. To explore the effects of H_2O in our calculation, we utilized two initial H_2O-contents: 0.5 wt% and 4 wt% to account for relatively dry and wet conditions. The oxygen chemical potential was controlled by imposing the FMQ buffer in all calculations.

Calculations were carried out at 0.25 GPa and 1 GPa, which approximate upper and lower crustal conditions, and were calculated isobarically over the temperature interval between 600 °C to the liquidus temperature (calculated by rhyolite-MELTS) in discrete steps. In rhyolite-MELTS, the FMQ buffer is not maintained below the solidus, and thus, results below such conditions are not discussed in this study.

Always consult and cite the final, published document. See http:/www.minsocam.org or GeoscienceWorld

This is the peer-reviewed, final accepted version for American Mineralogist, published by the Mineralogical Society of America.
The published version is subject to change. Cite as Authors (Year) Title. American Mineralogist, in press.
DOI: https://doi.org/10.2138/am-2022-8211. http://www.minsocam.org/

Comparison methodology

We performed a comparison using four sets of conditions. These include: (1) a low-*P*–low-H_2O run (i.e., at 0.25 GPa and 0.5 wt% H_2O), (2) a low-*P*–high-H_2O run (i.e., at 0.25 GPa and 4 wt% H_2O), (3) a high-*P*–low-H_2O run (i.e., at 1 GPa and 0.5 wt% H_2O), and (4) a high-*P*–low-H_2O run (i.e., at 1 GPa and 4 wt% H_2O). All calculations were carried out at discrete temperatures spanning the solidus to liquidus (or near-liquidus) temperatures along the selected pressures. As noted earlier, the equilibrium (closed system) states computed apply to both crystallization and melting, because at equilibrium, the liquid–solid–fluid relationships are the same for closed-system melting or crystallization. Thus, we emphasize that although the calculations (and Figs. 1, 2, and 4–7) proceed up temperature from near-soliuds toward near-liquidus (i.e., equilibrium partial melting), the calculations are equally applicable to down-temperature equilibrium crystallization since there is no fractionation of solids from liquid.

Because there are several versions of rhyolite-MELTS, we followed the decision tree on the rhyolite-MELTS website (http://melts.ofm-research.org/LIQUIDS-decision-tree.html) in order to choose the appropriate version for each calculation. All the rhyolite-MELTS runs were calculated with the version v1.2.0 with the exception of the low-*P*–high-H_2O run (i.e. at 0.25 GPa and 4 wt% H_2O), where v1.1.0 was used.

Phase modal proportions are shown using mode boxes, which include the calculated normalized mass proportions (wt%) of all predicted phases at each calculated state point (Figs. 1 and 2; mineral proportions in vol% are also shown in Supplementary Figures S1–S2). When more than one phase of the same solid solution were stable at a single state point (e.g., two clinopyroxenes predicted by rhyolite-MELTS), the phase masses were combined for simplicity. Calculated modal proportions are given in Table 2 every 100 °C from 900 (or 800 °C) to 1100

Always consult and cite the final, published document. See http:/www.minsocam.org or GeoscienceWorld

°C. The detailed description of the calculated phase equilibria evolution for the four scenarios is given in Appendix 1.

Liquid compositions are reported from the liquidus (calculated with rhyolite-MELTS) or near liquidus (HPx-mb16) to the solidus (Figs. 3–7). Given that the rhyolite-MELTS liquid *a–X* model, in contrast to the Green et al. (2016) liquid *a–X* model, considers both FeO and Fe_2O_3, the Fe content of the calculated compositions was recalculated to FeO^t allowing for direct comparison. Liquid compositions are given in Tables S2 and S3 every 100 °C from 900 (or 800 °C) to 1100 °C . Compositions are reported in the table only when liquid is stable in both rhyolite-MELTS and HPx-mb16 models at the same *P–T* conditions. The full liquid compositional evolution is described in Appendix 1.

In addition to providing a first-order comparison of the phase relations and liquid compositions, we also compare compositions of clinopyroxene, feldspar, orthopyroxene, amphibole and garnet, which are the most abundant minerals. A detailed description of the phase compositions at each state point can be found in the Appendix 1 and in Supplementary Figures S3–S6. Only the most signficant mineral-compositional differences and characteristics are presented and discussed in the sections below.

Models caveats

Both of the thermodynamic models used here (i.e., rhyolite-MELTS and HPx-b16) have significant caveats, limitations, and uncertainties, mainly related to the thermodynamic data and the *a–X* models. A detailed discussion is beyond the scope of this paper; the reader is referred to the original works and developers' websites to find important information related to the models (rhyolite-MELTS, http://melts.ofm-research.org; HPx-mb16, https://hpxeosandthermocalc.org).

Always consult and cite the final, published document. See http:/www.minsocam.org or GeoscienceWorld

Below, we only outline the calibration ranges where the thermodynamic models should yield reliable results and some important caveats pertinent to our comparison work.

Rhyolite-MELTS is recommended for modeling relatively dry mafic and hydrous silicic systems at < 2 GPa. Phase equilibria calculations via rhyolite-MELTS are not recommended at conditions close to the solidus (and subsolidus) and/or for intermediate and calc-alkaline systems with modally significant amphibole, muscovite, and biotite (http://melts.ofm-research.org; Gualda et al., 2012). Rhyolite-MELTS calculations are further recommended for volcanic systems where the melt fraction is > 50 wt% (Gualda et al., 2012).

Calculations with the HPx-mb16 model are recommended for modeling partial melting of hydrous metabasites at < 1.3 GPa. Reliable phase equilibria can be calculated at subsolidus and suprasolidus conditions up to ~1050 °C (Green et al., 2016; Palin et al., 2016); yet, modeling phase equilibria near- or at the liquidus is not recommended as the liquid *a–X* model accounts for neither Fe_2O_3 and TiO_2.

MODEL COMPARISON

Differences in the calculated phase proportions

Overall, rhyolite-MELTS calculates more liquid at higher temperatures (closer to the liquidus) but less liquid at lower temperatures (closer to the solidus) compared to HPx-mb16 (Figs. 1 and 2). For example, in the low-*P*–low-H_2O run at 1100 °C, rhyolite-MELTS predicts ~33 wt% liquid, whereas HPx-mb16 predicts ~50 wt% liquid (~36 vol% and ~53 vol%, respectively; Figs. 1a and c; Fig. S1a and c; Table 2). The position of the solidi vary depending on pressure between the two models as well. In the low-*P* runs, the solidus is located at higher temperature (e.g., ~850 °C vs ~730 °C in the high-H_2O run; Figs. 1b and d) whereas in the high-*P* run, it is located at

Always consult and cite the final, published document. See http:/www.minsocam.org or GeoscienceWorld

lower temperature (e.g., ~760 °C vs ~890 °C in the low-H_2O run; Figs. 2a and c) in rhyolite-MELTS compared to HPx-mb16. In all the calculations, a higher H_2O content decreases the solidus temperature (Figs. 1 and 2).

Clinopyroxene and plagioclase stabilities are expanded to higher temperatures in HPx-mb16 regardless of the conditions (Figs. 1 and 2). At temperatures closer to the solidus, rhyolite-MELTS predicts higher amounts of these phases, and the specific temperatures where rhyolite-MELTS predicts more of these phases depend on the specific run (Figs. 1 and 2; Table 2). For example, in the low-*P*–high-H_2O run at 900 °C, rhyolite-MELTS predicts ~32 wt% of clinopyroxene and ~27 wt% of plagioclase (~24 vol% and ~26 vol%, respectively), whereas HPx-mb16 predicts ~21 wt% clinopyroxene and ~22 wt% plagioclase (~16 vol% and ~21 vol%, respectively) (Figs. 1b and d; Fig. S1b and d; Table 2). Plagioclase proportion is systematically higher in rhyolite-MELTS at any given temperature in the low-*P* runs. For example, at 830 °C in the low-*P*–high-H_2O run, rhyolite-MELTS calculates ~46 wt% of plagioclase whereas HPx-mb16 predicts ~25 wt% (~43 vol% and ~25 vol%, respectively; Figs. 1b and d; Fig. S1b and d). By contrast, in the high-*P* runs, plagioclase systematics are different; in the low-H_2O run rhyolite-MELTS calculates less amount of plagioclase comapred to HPx-mb16, whereas in high-H_2O run, only HPx-mb16 predicts plagioclase (Fig. 2; Table 2).

Orthopyroxene and olivine proportions are systematically higher in the rhyolite-MELTS low-*P* runs compared to HPx-mb16 low-*P* runs (Fig. 1); olivine stability is typically expanded to higher temperatures in rhyolite-MELTS compared to HPx-mb16. In the low-*P*–low-H_2O run, olivine is not stable in rhyolite-MELTS but predicted in a small temperature window in the HPx-mb16 calculation (Fig. 1). By contrast, in the high-*P* runs, orthopyroxene and olivine are not stable except orthopyroxene only in the low-H_2O HPx-mb16 run.

Always consult and cite the final, published document. See http:/www.minsocam.org or GeoscienceWorld

This is the peer-reviewed, final accepted version for American Mineralogist, published by the Mineralogical Society of America.
The published version is subject to change. Cite as Authors (Year) Title. American Mineralogist, in press.
DOI: https://doi.org/10.2138/am-2022-8211. http://www.minsocam.org/

A crucial systematic difference at all *P*–*T*–H_2O conditions is the stability of amphibole. HPx-mb16 predicts amphibole in all runs; the amount of amphibole increases with increasing pressure and H_2O (Figs. 1c, 1d, 2c, and 2d; Table 2). By contrast, in the rhyolite-MELTS calculations, amphibole is only predicted in the high-*P*–high-H_2O run (Fig. 2b). The amount of amphibole, and its temperature-interval of stability, are not comparable with HPx-mb16 (Figs. 2b–d). For example, in the high-*P*–high-H_2O run at 700 °C, rhyolite-MELTS predicts ~2 wt% of amphibole compared to ~63 wt% in HPx-mb16 (~1 vol% and ~57 vol%, respectively; Figs. 2b and d; Fig. S2b and d). At 600 °C in the same run, the modal difference remains considerable: rhyolite-MELTS predicts ~22 wt% of amphibole whereas in HPx-mb16 modal amphibole is ~66 wt% (~20 vol% and ~61 vol%, respectively; Figs. 2b and d; Fig. S2b and d).

Garnet is only stable in the high-*P* runs in both models. Its stability is systematically expanded to higher temperature and the proportion is greater in rhyolite-MELTS compare to HPx-mb16 (Fig. 2). For instance, in the high-*P*–low-H_2O run at 800 °C, rhyolite-MELTS predicts ~32 wt% of garnet whereas HPx-mb16 predicts ~15 wt% (~27 vol% and ~12 vol%, respectively; Figs. 2a and c; Fig. S2a and c; Table 2). Unexpectedly, higher H_2O increases the proportion of garnet in rhyolite-MELTS (Figs. 2a and b). On the other hand, follows the opposite trend relative to H_2O (Figs. 2c and d), i.e., a higher H_2O ihibits garnet stabilizatin.

Other minor phases such as quartz and Fe-Ti oxides also show differences between the models (Figs. 1 and 2). Quartz is predicted at relatively similar temperatures (± 50 °C) but is systematically higher in proportion in rhyolite-MELTS in the low-H_2O runs but lower in the high-H_2O runs (Figs. 1 and 2). By contrast, proportions of Fe-Ti oxides are relatively similar (± 2 wt%), although the predicted phase is always different in the low-*P* runs: rhyolite-MELTS

Always consult and cite the final, published document. See http:/www.minsocam.org or GeoscienceWorld

predicts a spinel group phase (ulvospinel–magnetite) whereas HPx-mb16 predicts rutile that is replaced by ilmenite at lower temperature (Figs. 1 and 2).

The models predict H_2O-saturation conditions at different *P–T* conditions (Figs. 1 and 2). In the low-*P*–low-H_2O run, H_2O-saturated conditions are only attained in rhyolite-MELTS (Fig. 1a). By contrast, in the low-*P*–high-H_2O run, all calculations reach H_2O-saturated conditions, although H_2O as a phase occurs at higher temperatures and in lower proportion in HPx-mb16 (Figs. 1b and d). In the small temperature interval where H_2O is in excess in HPx-mb16 but not in rhyolite-MELTS (i.e., ~1100–1000 °C; Figs. 1b and d), the liquid proportion is higher in rhyolite-MELTS (Figs. 1b and d). In the high-*P* runs, H_2O-saturated conditions are only reached in the high-H_2O run in both models (Figs. 2b and d). Similar to the low-*P* runs, H_2O occurs at slightly higher temperatures in HPx-mb16 runs (Figs. 2b and d).

In all our calculations, there are four phases that are only stable in either rhyolite-MELTS or in HPx-mb16. These are analcime (only predicted by rhyolite-MELTS) and epidote, titanite, and rutile (only predicted by HPx-mb16). (Figs. 1 and 2).

Differences in the calculated phase compositions

Liquid compositions. The calculated silicate liquids follow relatively similar compositional trends as a function of temperature (Fig. 3); changes in liquid composition are controlled by the crystallization or consumption of phases which, as noted above, differ between models.

Generally, high-*T* liquid compositions are relatively similar in SiO_2 but for most calculations, diverge at lower temperatures. In the low-*P*–low-H_2O run, where the SiO_2 is enriched in HPx-mb16 at high temperatures compared to the liquid predicted by rhyolite-MELTS (Fig. 4a). At lower temperatures in the low-H_2O runs, HPx-mb16 liquid compositions are SiO_2-

Always consult and cite the final, published document. See http:/www.minsocam.org or GeoscienceWorld

This is the peer-reviewed, final accepted version for American Mineralogist, published by the Mineralogical Society of America.
The published version is subject to change. Cite as Authors (Year) Title. American Mineralogist, in press.
DOI: https://doi.org/10.2138/am-2022-8211. http://www.minsocam.org/

367 depleted compared to rhyolite-MELTS (up to ~5 wt%; Figs. 4a and 6a); by contrast, in the high-
368 H_2O runs, the HPx-mb16 liquid compositions are SiO_2-enriched compared to rhyolite-MELTS
369 (up to ~16 wt%; Figs. 5a and 7a). The liquid SiO_2 contents in the low-*P*–high-H_2O runs in
370 rhyolite-MELTS and HPx-mb16 are almost identical (Fig. 5a)

371 Calculated liquids are systematically—and substantially—more mafic in the HPx-mb16
372 than in rhyolite-MELTS (up to ~18 wt% higher in the high-*P*–low-H_2O run at 1080°C; Fig. 6c).
373 Liquid FeO^t + MgO in HPx-mb16 shows a distinct enrichment at high temperatures that is not
374 observed in rhyolite-MELTS (Figs. 4c, 5c, 6c, and 7c). These changes are less significant as the
375 H_2O content increases at the same pressure (Figs. 4c and 5c); the high-*P*–high-H_2O run show the
376 least difference in liquid FeO^t + MgO (Fig. 7c).

377 The liquid CaO and H_2O contents have similar compostional trends in both models, and
378 tend to be higher in rhyolite-MELTS. The relative difference in the CaO and H_2O contents is
379 greater in the low-*P* runs (up to 5 wt% in Cao and ~4 wt% in H_2O Figs. 4f and 5f); by contrast,
380 in the high-*P* runs, the difference in the liquid CaO and H_2O content is smaller (Figs. 6f and 7f).
381 In all the runs, the H_2O liquid content tend to diverge the most at lower temperatures (Figs. 4f,
382 5f, 6f, and 7f).

383 Liquid Al_2O_3 and alkali contents are relatively different between the models throughout.
384 The liquid Al_2O_3 content follow different trends in all the runs (Figs. 4b, 5b, 6b, and 7b); the
385 alkali content are relatively similar in all the low-*P* runs (Figs. 4d and 5d). In the high-*P* runs,
386 within 1200–900 °C (in the low-H_2O content run) and 1100–750 °C (in the high-H_2O content
387 run), rhyolite-MELTS calculated liquid compostion is greater in the alkali contents compared to
388 the HPx-mb16 liquid composition (up to 2–3 wt%; Figs. 6d and 7d).

Always consult and cite the final, published document. See http:/www.minsocam.org or GeoscienceWorld

Overall, liquid compositions show the greatest difference at lower temperatures, closer to the solidus: the low-*P* runs are the most similar (especially CaO and alkalis; Figs. 4 and 5), whereas in the high-*P* runs, compositional differences are more distinct (especially in the case of SiO_2, Al_2O_3, and H_2O; Figs. 6 and 7).

Mineral compositions. Details of the mineral chemical evolution and the results derived from both models can be found in Appendix 1 and in the Supplemenatary Figures S2–S5. Among the most important differences is that the clinopyroxene shows similar Mg# [Mg# = Mg/(Fe^{2+} + Mg)] at temperatures near the liquidus, but with decreasing temperature, rhyolite-MELTS predicts higher clinopyroxene Mg# values compared to HPx-mb16 in all runs. Plagioclase anorthite content is systematically higher in HPx-mb16 at any temperature compared to rhyolite-MELTS in all the runs. In the high-*P* runs, garnet Mg# values are systematically higher in rhyolite-MELTS compared to HPx-mb16 at any given temperature; almandine and grossular contents are systematically higher and pyrope contents lower in HPx-mb16. Calculated amphibole compositions are substantially different between rhyolite-MELTS and HPx-mb16, reflecting the complexity and difficulty modeling *a*–*X* relations in multisite-multicomponent amphibole phases using available experimental data (Supplementary Table S4). The Si, Mg# and Ca contents are systematically higher in rhyolite-MELTS than in HPx-mb16 at any given temperature in the high-*P*–high-H_2O run.

TRACE-ELEMENT SIGNATURES OF MODEL LIQUIDS

Here, we explore the effect of calculated phase relations on the trace-element signatures of the liquids. We used calculated liquid and solid fractions (Supplementary Table S5) along with

Always consult and cite the final, published document. See http:/www.minsocam.org or GeoscienceWorld

This is the peer-reviewed, final accepted version for American Mineralogist, published by the Mineralogical Society of America.
The published version is subject to change. Cite as Authors (Year) Title. American Mineralogist, in press.
DOI: https://doi.org/10.2138/am-2022-8211. http://www.minsocam.org/

412 liquid–mineral partition coefficients to model the liquid trace-element signatures at (1) 900 °C in
413 the low-*P*–low-H_2O run, (2) 1000 °C in the high-*P*–low-H_2O run, and (3) 850 °C in the high-*P*–
414 high-H_2O run. These three scenarios were selected because of the markedly different predicted
415 equilibria between the models. Trace-element modeling was performed at the given state point
416 using mass balance equations found elsewhere (e.g., Shaw, 2006; Spera et al*.,* 2007). A wide
417 selection of variably incompatible trace elements was chosen, and partition coefficients were
418 from Bédard (2006) (Supplementary Table S6). To highlight the similarities and differences in
419 trace element signatures resulting solely from phase assemblage differences, constant liquid–
420 mineral partition coefficients (for each mineral) were used. The starting bulk trace-element
421 composition was that of mean N-MORB from Gale et al. (2013). The results are given in Table 3
422 and illustrated in normalized incompatible trace-element diagrams and REE diagrams in Figure
423 8.

424 In the low-*P*–low-H_2O run at 900 °C, the stable phase assemblage predicted by rhyolite-
425 MELTS is liquid–plagioclase–orthopyroxene–clinopyroxene–magnetite (Fig. 1c). The calculated
426 liquid trace-element pattern (Figures 8a and b) is relatively enriched in Ta and Zr, and depleted
427 in Ba, Pb, Sr, Eu, and Ti. The liquid composition is further characterized by a low Sr/Y ratio
428 (Sr/Y = 0.44; Table 3), and is not strongly fractionated in REE (La/Yb = 1.86; Table 3). The
429 chondrite-normalized REE pattern shows a strong negative Eu anomaly (Eu/Eu* = [Eu/(Sm x
430 $Nd)^{0.5}$] = 0.07; Table 3), and is characterized by a flat heavy-REE (HREE) slope (Yb/Gd = 0.62;
431 Table 6). The calculated paragenesis using HPx-mb16 is liquid–plagioclase–amphibole–
432 orthopyroxene–clinopyroxene–ilmenite (Fig. 1c). While the HPx-mb16 liquid compositions
433 show relatively lower concentrations of all the considered trace elements, most of trace elements
434 are similar to those calculated with rhyolite-MELTS. Exceptions are Ta, Gd and Tb which are

Always consult and cite the final, published document. See http:/www.minsocam.org or GeoscienceWorld

much lower in concentration in HPx-mb16. The liquid composition is characterized by low Sr/Y (Sr/Y = 0.76) and La/Yb (La/Yb = 2.26) ratios (Table 3), a strong Eu negative anomaly (Eu/Eu* = 0.12; Table 3), and a flat HREE slope (Yb/Gd = 0.78; Table 3).

In the high-*P*–low-H_2O run, the stable phase assemblage at 1000°C for the rhyolite-MELTS run is liquid–plagioclase–clinopyroxene–garnet (Fig. 2c). The calculated trace-element compositions are shown in Figures 8c and d.The liquid incompatible trace-element pattern is slightly enriched in Ta and Ti but depleted in Ba and Sr, and further characterized by a moderate Sr/Y ratio (Sr/Y = 10.93; Table 3). It is also strongly fractionated in light to heavy REE (La/Yb = 35.24; Table 3) because garnet is a stable phase. The REE pattern does not show a negative Eu anomaly (Eu/Eu* = 0.30; Table 3), and is characterized by a steep HREE slope (Yb/Gd = 0.18; Table 3). The paragenesis in HPx-mb16 is liquid–plagioclase–amphibole–orthopyroxene–clinopyroxene–ilmenite (Fig. 2c). The incompatible trace-element pattern of HPx-mb16 is similar to that of rhyolite-MELTS for highly incompatible elements, but there are significant differences in terms of Eu, Gd, Ta, and HREE; the liquid composition is also characterized by a low Sr/Y ratio (Sr/Y = 0.80; Table 3). The REE pattern is not fractionated (La/Yb = 2.12; Table 6), shows a strong negative Eu anomaly (Eu/Eu* = 0.12; Table 3), and is enriched in HREE (Yb/Gd = 0.72; Table 3).

In the high-*P*–high-H_2O run at 850 °C, the paragenesis predicted by MELTS is liquid–clinopyroxene–garnet (Fig. 2d). The calculated trace-element compositions are shown in Figures 8e and f. The calculated incompatible trace-element pattern is slightly enriched in Pb, Sr, and Ti and slightly depleted in Th. The liquid composition has a high Sr/Y ratio (Sr/Y = 142.48; Table 3) and is strongly fractionated in LREE/HREE (La/Yb = 74.96; Table 3) due to residual garnet. The REE pattern further shows a small positive Eu anomaly (Eu/Eu* = 0.48; Table 3), and is

Always consult and cite the final, published document. See http:/www.minsocam.org or GeoscienceWorld

458 characterized by a steep HREE slope (Yb/Gd = 0.17; Table 3). The calculated paragenesis in
459 HPx-mb16 is liquid–amphibole–orthopyroxene–clinopyroxene–garnet–titanite (Fig. 2d). The
460 incompatible trace-element pattern is depleted in highly incompatible elements but enriched in
461 more compatible elements relative to that of the rhyolite-MELTS liquid. The pattern is further
462 characterized by a slight enrichment in Pb, Sr, and Zr and depletion in Ti; the liquid composition
463 has a moderate Sr/Y ratio (Sr/Y = 12.07; Table 3). The REE pattern is not fractionated (La/Yb =
464 3.54; Table 3), does not show an Eu negative anomaly (Eu/Eu* = 0.37; Table 3), and is enriched
465 in HREE (Yb/Gd = 0.81; Table 3).
466
467 **Contrasting liquid trace-element signatures: the effect of contrasting mineral assemblages**
468 As discussed in the previous sections, both models yield significant differences in calculated
469 phases and their relative abundances. Unsurprisingly, this directly affects the trace-element
470 signatures of the liquids. For example, partitioning of Ba, Sr, and Eu into plagioclase (Gromet
471 and Silver, 1983), means that the increase of plagioclase stability at higher temperatures in HPx-
472 mb16 relative to rhyolite-MELTS and the differences in plagioclase proportion will lead to
473 differences in the concentrations of the Ba, Sr, and Eu in liquids in equilibrium with their
474 associated crystals at each state point (Fig. 8; Table 3). The considerable effect of the discordant
475 phase equilibria on the trace-element budget is also well illustrated by the contrasting garnet
476 stabilities in the different models. Garnet is more stable in all rhyolite-MELTS calculations, and
477 since it is an important HREE repository (e.g., Bea et al., 1994), its fractionation causes notable
478 HREE depletions in the corresponding rhyolite-MELTS liquid compositions (Fig. 8; Table 3).
479 The HPx-mb16 trace-element patterns always show negative Ti anomalies, whereas
480 trace-element patterns of rhyolite-MELTS calculations only show negative Ti anomalies in the

Always consult and cite the final, published document. See http:/www.minsocam.org or GeoscienceWorld

high-*P*–low-H_2O case (Fig. 8; Table 3). The negative Ti anomalies in HPx-mb16 trace-element patterns are controlled by partitioning of Ti into titanite, ilmenite, and amphibole (where present), whereas such phases are never stable in rhyolite-MELTS calculations. In the only example where there is a negative Ti anomaly (Fig. 8; Table 3) in rhyolite-MELTS, the main Ti repository is magnetite.

A key difference in the mineral assemblage predicted by rhyolite-MELTS and HPx-mb16 models is the presence of amphibole. This mineral has relatively high partition coefficients for MREE and HREE (Table S6; Bédard, 2006) likely accounting for the depletition in MREE and HREE contents in amphibole-rich HPx-mb16 calculations compared to those of rhyolite-MELTS, as well as to HPx-mb16 calculations with less amphibole (Fig. 8; Table 3).

Other trace elements (e.g., Cs, Rb, Th, U, and light-REE) are mainly incompatible to the solid phases present in the calculations, thus the concentrations in the melt are only slightly affected by the choice of the thermodynamic model (Fig. 8; Table 3). Rather subtle relative differences in their concentrations can be observed in the high-*P*–high-H_2O run (Fig. 8; Table 3). Highly incompatible elements may thus generally represent better proxies to model crystallization or anatectic processes with both rhyolite-MELTS and HPx-mb16, since they are less prone to differ significantly with model choice.

COMPARING MODELS TO PETROLOGICAL EXPERIMENTS

To further assess the robustness of the phase equilibria models, we compared model predictions with results from low- and high-*P* petrological experiments. We selected the experimental studies of Berndt et al. (2005) and Sen and Dunn (1994) as benchmarks for the comparison. We used the synthetic MORB B1 composition from Berndt et al. (2005) and compared the phase

Always consult and cite the final, published document. See http:/www.minsocam.org or GeoscienceWorld

equilibria at 0.2 GPa and 950 °C and 1000 °C. These conditions correspond to their runs 148 and 153 (their Table 3c). The data in Berndt et al. (2005) were not used in either rhyolite-MELTS or HPx-mb16 calibrations. In addition, we utilized the natural basaltic amphibolite from the Sen and Dunn (1994) experiment and compared the phase equilibria at 1.5 GPa and 975 °C and 1025 °C. These conditions correspond to their runs B17 and M2 (their Table 2). Although data from Sen and Dunn (1994) were not used to calibrate HPx-mb16, Sen and Dunn data did form a very small part of the data used to calibrate rhyolite-MELTS (Ghiorso et al., 2002). The Berndt et al. (2005) experiments considered oxygen fugacities corresponding to the FMQ buffer whereas the Sen and Dunn (1994) oxygen fugacity corresponds to FMQ = + 0.5. Here, for simplicity, calculations with both rhyolite-MELTS and HPx-mb16 where run along the FMQ buffer. Phase proportions from the Berndt et al. (2005) and Sen and Dunn (1994) experiments as well as phase equilibria calculations with rhyolite-MELTS (v1.2.0) and HPx-mb16 are shown in Figure 9 and given in Table 4; experimental and calculated liquid compositions are given in Table 5.

MORB B1 of Berndt et al. (2005)

Phase equilibria at 950 °C slightly differs between the models and experiment 153 (Fig. 9a; Table 4). Liquid–olivine–clinopyroxene–plagioclase–amphibole–H_2O is the observed paragenesis in the experiment. Rhyolite-MELTS differs from the experiment in that it stabilizes orthopyroxene and a small amount of magnetite but not amphibole. HPx-mb16 stabilizes amphibole, clinopyroxene, and plagioclase as in the experiment but with additional orthopyroxene and a small amount of ilmenite and no olivine. The liquid proportion in the experiment is similar to that predicted in HPx-mb16 but significantly lower in rhyolite-MELTS. Clinopyroxene and plagioclase proportions are relatively similar in HPx-mb16 compared to the

Always consult and cite the final, published document. See http:/www.minsocam.org or GeoscienceWorld

experiment; rhyolite-MELTS predicts higher proportions of these phases than both HPx-mb16 and the experiment. The olivine proportion is higher in the rhyolite-MELTS model compared to the experiment. On the other hand, the proportion of amphibole observed in the experiment is similar to that predicted by HPx-mb16. In general, HPx-mb16 is able to better reproduce the phase relations from the experiment 153. The rhyolite-MELTS liquid composition is relatively similar to that of the experiment in terms of MgO and CaO contents whereas the HPx-mb16 liquid composition is in relative agreement with regards to all the other major oxides (Table 5). Significant differences include the MgO and K_2O contents; for instance, the liquid's MgO content in rhyolite-MELTS is within ~5% of the experiment whereas the K_2O content is within ~382% of the experiment. By contrast, the the HPx-mb16 calculated MgO content is within ~115% of the experiment whereas the K_2O content is within ~74% of the experiment. Note that the large relative difference in the K_2O content is exacerbated by low K_2O contents.

At 1000 °C, the rhyolite-MELTS and HPx-mb16 models, and the experiment 148 of Berndt et al. (2005) show the same phase assemblage, melt–olivine–clinopyroxene–plagioclase–H_2O, with the exception of a very small amount of ilmenite that is predicted in HPx-mb16. However, the phase proportions are somewhat different (Fig. 9b; Table 4); both rhyolite-MELTS and HPx-mb16 predict considerably less liquid than observed in the experiment, and both models predict more plagioclase. Rhyolite-MELTS predicts slightly more olivine than measured in the experiment whereas the HPx-mb16 predicts slightly less olivine than in the experiment. Modeled and experimental clinopyroxene proportions are similar. Overall, rhyolite-MELTS is able to better reproduce the phase equilibria from experiment 148. The HPx-mb16 calcualted liquid composition is relatively similar to that of the experiment in terms of SiO_2, Al_2O_3, and H_2O contents, whereas the rhyolite-MELTS liquid composition is in reasonable agreement with the

Always consult and cite the final, published document. See http:/www.minsocam.org or GeoscienceWorld

experiment for all the other major oxides (Table 5). Important differences in the compositions include the MgO and K_2O contents; for example, the MgO liquid content in rhyolite-MELTS is within ~3% of the experiment whereas the liquid's K_2O content is within ~38% of the experiment. On the other hand, the HPx-mb16 calculated liquid MgO content is within ~74% of the experiment and the K_2O content within ~51% of the experiment.

Natural basaltic amphibolite of Sen and Dunn (1994)

The stable phase assemblage in the 975 °C experiment M2 is liquid–clinopyroxene–plagioclase–amphibole–garnet–rutile. Rhyolite-MELTS model does not stabilize plagioclase, amphibole, or rutile, whereas HPx-mb16 stabilizes the same experimental phase assemblage with the exception of plagioclase (Fig. 9c; Table 4). Phase proportions are relatively different between both models and the experiment; the calculated liquid fractions are considerably higher than in the experiment. The calculated clinopyroxene proportion in HPx-mb16 is similar to that in the experiment but considerably higher in rhyolite-MELTS. Similarly, the garnet proportions predicted by both models are significantly higher than in the experiment. The calculated amphibole proportion in HPx-mb16 is relatively less than in the experiment. Rutile occurs as minor phase in both HPx-mb16 and the experiment. In general, HPx-mb16 better reproduces the phase relations at 975 °C. The rhyolite-MELTS liquid composition is relatively similar to that of the experiment in terms of FeO^t and MgO liquid contents whereas the HPx-mb16 liquid composition is in relative agreement with the experiment for all the other major oxides (Table 5). Significant differences include the FeO^t and K_2O contents; for instance, the FeO^t liquid content in rhyolite-MELTS is within ~29% of the experiment whereas the liquid K_2O content is within

Always consult and cite the final, published document. See http:/www.minsocam.org or GeoscienceWorld

572 ~86% of the experiment. On the other hand, the HPx-mb16 calculated FeO^t liquid content is
573 within ~73% of the experiment and the K_2O content is within ~32% of the experiment.
574 The observed paragenesis at 1025 °C in the Sen and Dunn (1994) experiment B17 is
575 liquid–clinopyroxene–amphibole–garnet–rutile. HPx-mb16 predicts the same phases, whereas
576 rhyolite-MELTS differs from the experiment in that it stabilizes neither amphibole nor rutile.
577 Proportions of most other phases are fairly similar between the computed models and the
578 experiment, although HPx-mb16 predicts relatively more liquid and less clinopyroxene (Fig. 9d;
579 Table 4). The proportion of garnet calculated with rhyolite-MELTS is considerably higher than
580 in the experiment, whereas HPx-mb16 predicts a relatively higher amount of garnet. The
581 amphibole proportion observed in the experiment is similar to that predicted by HPx-mb16.
582 Rutile occurs as a minor phase in both HPx-mb16 and the experiment. In general, HPx-mb16
583 better reproduces the phase relations of the experiment M2. The rhyolite-MELTS liquid
584 composition is relatively similar to that of the experiment in terms of SiO_2, FeO^t, and MgO
585 contents, whereas the HPx-mb16 liquid composition is in relative agreement with all other major
586 element oxides (Table 5). Important differences include the FeO^t and Na_2O contents; for
587 example, the FeO^t liquid content in rhyolite-MELTS is within ~32% of the experiment whereas
588 the liquid Na_2O content is within ~79% of the experiment. By contrast, the HPx-mb16 calculated
589 FeO^t is within ~78% of the experiment and the liquid's Na_2O content within ~1% of the
590 experiment.
591

592 **DISCUSSION**

593 Although a minor oxide and therefore not as important as many of the major element oxides, the
594 lack of the TiO_2 component in the Green et al. (2016) liquid *a–X* relations precludes accurately

Always consult and cite the final, published document. See http:/www.minsocam.org or GeoscienceWorld

595 modeling phase equilibria at or near liquidus conditions using HPx-mb16 in the NCKFMASHTO
596 system. As TiO_2 cannot be incorporated into the liquid, there is always a Ti-bearing stable phase
597 at high-*T*; this, in turn, affects the overall phase equilibria incluing the liquid compositions. For
598 instance, rhyolite-MELTS predicts the liquidus at ~1340–1100 °C, whereas in the HPx-mb16
599 model is unable to model these conditions; clinopyroxene and/or plagioclase, and a Ti-bearing
600 phase are already present at the liquidus conditions predicted by rhyolite-MELTS (Figs. 1 and 2).
601 Recently, Holland et al. (2018) and Tomlinson and Holland (2021) published *a–X* relations for
602 relevant crystalline solutions enabling modeling of peridotitic to granitic liquids. This set of *a–X*
603 relations includes more complex liquid and clinopyroxene *a–X* relations (including TiO_2 and
604 Fe_2O_3 in the liquid, and TiO_2 and K_2O in the clinopyroxene) than in the *a–X* relations from HPx-
605 mb16. In the first instance, this set of *a–X* relations might represent a better approach to
606 modeling suprasolidus processes than HPx-mb16; yet, a recent study indicates that phase
607 equilibria calculated with the Holland et al. (2018) relations are not significantly different from
608 calculations performed with HPx-mb16; moreover, HPx-mb16 produces similar compositions
609 and better reproduces the FeO^t and MgO liquid contents from experiments than the Holland et al.
610 (2018) *a–X* relations (García-Arias, 2020).

611 When comparing our model predictions to experiments, rhyolite-MELTS and HPx-mb16
612 better reproduce phase equilibria within the *P–T* conditions in which they were calibrated to be
613 used. The phase equilibria predicted by rhyolite-MELTS are broadly similar to the high-*T*
614 experiments compared to those predicted by HPx-mb16 (Fig. 9; Tables 4 and 5); by contrast, at
615 temperatures less than ~1000 °C, HPx-mb16 provides more robust liquid-present phase
616 equilibria (Fig. 9; Tables 4 and 5) as it better reproduces the considered experiments compared to

Always consult and cite the final, published document. See http:/www.minsocam.org or GeoscienceWorld

rhyolite-MELTS. Importantly, as shown in some works (e.g. White et al., 2007; Green et al., 2016), HPx-mb16 is able to accurately capture subsolidus equilibria.

One of the key differences between the rhyolite-MELTS and HPx-mb16 models is how H_2O is partitioned in the liquid and hydroxyl (OH^-) in the crystalline phases. Amphibole is predicted in HPx-mb16 calculations whereas amphibole stability and modal abundance are quite limited in rhyolite-MELTS (Figs. 1 and 2; Table 2). In the calculations presented here, rhyolite-MELTS partitions H_2O into liquid and/or analcime and/or a coexisting fluid phase (Figs. 1 and 2; Table 2). These results illustrate the acknowledged limitation of rhyolite-MELTS in modeling amphibole (and biotite)-bearing phase equilibria (http://melts.ofm-research.org/; Ghiorso and Gualda, 2015). The HPx-mb16 model may therefore be the best choice to model equilibrium melting and crystallization in scenarios where significant amounts of modal amphibole are observed or predicted.

While not considered in our present study, the use of the HPx-mb16 model to study fractional crystallization or any other open-system process would be relatively laborious for this task with the current software available (i.e., Theriak-Domino, Perple_X, and THERMOCALC), although several works using these software have succesfully modeled open-system processes (e.g., Yakymchuk and Brown, 2014; Kendrick and Yakymchuk, 2020; Stuck and Diener, 2020; Johnson et al., 2021; Hernández-Montenegro et al., 2021)

Furthermore, it is important to note that recent comparative study assessing the robustness of the Green et al. (2016) clinopyroxene and amphibole a–X relations shows discrepancies between the phase equilibria calculations and natural rocks in the proportions and compositions (Forshaw et al., 2019; Santos et al., 2019); yet, our comparisons with the experiments show that the difference in proportions are not as significant as suggested in those

Always consult and cite the final, published document. See http:/www.minsocam.org or GeoscienceWorld

640 studies. We argue that these different outcomes may be related to different bulk-rock
641 compositions used in the comparisons.
642
643 **IMPLICATIONS**
644 From the examples presented here, the lesson is clear: the modeling tool choice, and an
645 understanding of model constraints, uncertainties, and the similarities (and differences) among
646 models are critical to accruately convey the geological implications of a computational result.
647 Below, we highlight selected examples of how model choice can influence geologic
648 interpretations. The examples cited below are illustrative since we only present a small subset of
649 possible compositions and conditions, and yet, the underlying principal conclusion likely
650 remains relevant to all model-based studies of the magmatic evolution of the crust and upper
651 mantle.
652 HPx-mb16 and rhyolite-MELTS yield distinctly different minerals assemblages for some
653 of the runs. For example, at 850 °C in the low-*P*–high-H_2O run, the crystalline phases in
654 equilibrium with liquid predicted by rhyolite-MELTS correspond to a granulitic assemblage
655 whereas in HPx-mb16, an amphibolite-like assemblage is predicted (Figs. 1b and d). Similarly,
656 at 800 °C in the high-*P*–low-H_2O run, rhyolite-MELTS predicts a plagioclase-bearing garnet
657 pyroxenite crystalline assemblage whereas HPx-mb16 predicts a garnet amphibolite crystalline
658 assemblage (Figs. 2a and c; Table 2). As a consequence of the difference in amphibole stability,
659 the distribution of H_2O content among solid phases is different depending on the modeling tool.
660 This has important implications for modeling crustal anatexis and growth processes. For
661 example, the fertility (i.e., the potential to melt) of these solid assemblages will differ
662 significantly; amphibole dehydration melting of the amphibolitic cumulate would promote

Always consult and cite the final, published document. See http:/www.minsocam.org or GeoscienceWorld

663 greater liquid fractions (for the same pressure and temperature conditions) compared to the dry
664 granulitic and/or pyroxenite cumulate; different modeling approaches will lead to different
665 volumes of liquid, and thus in different crustal growth rates. The differences of the calculated
666 phases can also affect petrophysical properties such as density, seismic velocities, and thermal
667 conductivity (e.g., Carlson and Miller, 2004; Whittington et al, 2009). For example, at 900 °C in
668 the high-*P*–high-H_2O run (Figs. 2a and c; Table 2), the dry crystalline assemblage predicted by
669 rhyolite-MELTS (i.e., the garnet pyroxenite) has a significantly higher density (ρ = 3.59 g/cm^3)
670 than the hydrated mineral assemblage predicted by the HPx-mb16 model (ρ = 2.82 g/cm^3); such
671 differences may influence interpretations invoking crustal foundering via gravitational
672 instabilities which in turn may drastically affect the compositional stratification of the crust.
673 Differences in thermal diffusivity would also be expected between the hydrous and anhydrous
674 mineral assemblages, which would affect heat flow and the associated local geotherms. Thus, the
675 choice of modeling approach may yield different intepreretations for the development of
676 chemical stratification of continental crust, the potential for crustal delamination, and the thermal
677 and rheological crustal structure.

678 Observed differences between the calculated liquid compositions may have important
679 implications for forward modeling of igneous processes. For instance, different calculated melt
680 compositions may lead to distinct liquid lines of descent representing different magma series
681 (Fig. 3; e.g., Carmichael et al, 1974). In the low-*P*–high-H_2O run, the HPx-mb16 liquid
682 composition produced by equilibrium crystallization follows a subalkaline tholeiitic trend
683 whereas the liquid calculated with rhyolite-MELTS evolves first along a subalkaline trend but
684 then follows an alkaline series trend when equilibrium crystallization is greater than 50%
685 complete (Fig. 3b). These model differences could lead to differences in, for example,

Always consult and cite the final, published document. See http:/www.minsocam.org or GeoscienceWorld

686 hypotheses about tectonic setting. Furthermore, our results show that calculated liquid
687 compositions diverge more at near-solidus temperatures, the difference being greater in the high-
688 *P* calculations (Fig. 3). These differences have implications for modeling processes such as
689 crustal assimilation because the composition of small degree (near solidus) anatectic melts can
690 have profound impact on the major and trace element, isotopic, and phase equilibria signatures of
691 crustally contaminated magmas (e.g., Bohrson et al., 2014). Our results therefore concur with the
692 recognized limitation of thermodynamic modeling at "lower" temperatures, particularly using
693 rhyolite-MELTS (http://melts.ofm-research.org/) (e.g., rhyolite-MELTS is suggested to perform
694 best when a silicate liquid is present in the phase assemblage, as illustrated in the comparison
695 with the experiments (Fig. 9; Tables 4 and 5).

696 The difference in the calculated liquid compositions coupled with the calculated solid
697 fractions may significantly impact interpretation of tonalite-trondhjemite-granodiorite (TTGs)
698 and adakite petrogenesis. The major elements commonly used to identify and classify TTGs and
699 adakites (e.g., high Mg# and low K_2O/Na_2O) are some of the elements that vary the most
700 between the models. (Figs. 4–7), complicating their use in documenting the petrogenesis of such
701 rocks (e.g. Moyen, 2011; Palin et al., 2016; Hernández-Uribe et al., 2020). The solid assemblage
702 controls the trace-element liquid signature, which has been considered diagnostic of the source
703 depth and composition of the liquid (Moyen and Martin, 2012). TTGs are subdivided into high-,
704 medium-, and low-pressure groups based on the Sr/Y and La/Yb ratios, which are controlled by
705 garnet, plagioclase, rutile, and amphibole stabilities (Moyen, 2011; Moyen and Martin, 2012).
706 According to our results, the presence or absence, and abundace of such phases may vary
707 substantially between the two thermodynamic models examined here (Figs. 1 and 2; Table 2).
708 For example, garnet stability is increased in rhyolite-MELTS compared to HPx-mb16, whereas

Always consult and cite the final, published document. See http:/www.minsocam.org or GeoscienceWorld

plagioclase stability is expanded to higher temperatures in HPx-mb16 but generally predicted in lower proportions (Figs. 1 and 2). Such differences could easily lead to contrasting trace-element signatures (Table 3) and thus result in different explanations for tectonic environments of formation for TTGs (e.g., slab melting during subduction vs. melting of a thickened crust; Martin et al., 2014; Palin et al., 2016; Johnson et al., 2017). This emphasizes the need for careful consideration of model limitations and uncertainties.

Statements about model performance are nuanced and must be thoughtfully considered depending on the particular application under study, including the inherent geological uncertainties not associated with the thermodynamic model *per se*. There may be cases where the geological uncertainties are larger than the model uncertainties or vice versa. A careful parsing of all uncertainties—intermodel, intramodel and geologic—is critical when applying thermodynamic models to Earth systems.

The comparisons presented in this study are illustrative not exhaustive. We performed equilibrium modeling using a single bulk composition (N-MORB) over a modest range of pressures and bulk H_2O contents. We did not consider fractional or open-system processes, nor other redox conditions; such comparisons are outside of the scope of a single paper. In felsic and/or open systems, which often show considerably higher degrees of geochemical heterogeneity, the differences between the models may be larger, especially when amphibole and sheet silicate crystalline solutions are more abundant. We hope our work spurs additional work including further comparative examination of other thermodynamic conditions (composition, volatiles, redox, pressure, phase assemblages) and models.

From our limited set of comparative calculations, there are three major points. The first is that our results show how the choice of petrological modeling tool can influence conclusions

Always consult and cite the final, published document. See http:/www.minsocam.org or GeoscienceWorld

about associated geological processes. We have shown that for the same model input (e.g., *P–T–*H_2O), model choice may lead to different intepretations of crustal structure, density, and melting systematics. The second point is that different models are better suited to modeling different *P–T* ranges, and that studies such as ours are needed to highlight these differences for users more comprehensively. For example, HPx-mb16 is likely better suited for modeling water-rich systems with hydrous mineral phases (e.g., volcanic arc settings) at lower temperatures, whereas rhyolite-MELTS may work better for drier systems at lower pressures and higher temperatures (e.g., MORB and OIB's). Third, our work illustrates the importance of using mutiple petrological indicators to assess the efficacy of one model versus another. Major- and trace-element and isotopic compositions of mineral phases as well as mineral proportions can enhance the choice of a best-fit model compared to using melt compostional data only.

While the current thermodynamic databases and *a–X* relations for solid-solution phases used in the igneous and metamorphic petrology communities provide a framework for forward modeling of important igneous and metamorphic processes, the ultimate goal should be to develop an internally consistent thermodynamic database and *a–X* relations applicable to both subsolidus metamorphic processes as well as suprasolidus igneous and metamorphic processes. This methodological development should proceed hand-in-hand with new petrological experiments that fill the current gap in knowledge (especially at high pressure conditions) and with a development of a user-friendly software with the capability to model the range of closed and open-system processes that are relevant to igneous and metamorphic systems (e.g., equilibrium/fractional melting/crystallization and crustal assimilation). In parallel with model development and enhancement, systematic comparative studies—such as the one presented here—are necessary to thoroughly assess and test predictions from different models and to

Always consult and cite the final, published document. See http:/www.minsocam.org or GeoscienceWorld

755 compare to experimental and natural data. We hope our study provokes others to continue to
756 explore the strengths and weaknesses of the available multicomponent and multiphase phase
757 equilibria tools.
758
759 **ACKNOWLEDGMENTS**
760 D. Hernández-Uribe thanks M. Konrad-Schmölke and J. D. Hernández-Montenegro for help
761 with Theriak-Domino calculations. F. J. Spera acknowledges the support of the U.S. National
762 Science Foundation over the past fifty years. W. A. Bohrson received funding for this project
763 from the U. S. National Science Foundation and the Colorado School of Mines. The contribution
764 of J. S. Heinonen was supported by the Academy of Finland Grant 295129. Reviews by J. Brian
765 Balta and J. Diener greatly improved the manuscript and are gratefully acknowledged. A.
766 Acosta-Vigil is thanked for editorial handling.
767
768 **REFERENCES**
769 Asimow, P. D., and Ghiorso, M. S. (1998) Algorithmic modifications extending MELTS to
770 calculate subsolidus phase relations. American Mineralogist, 83, 1127–1132.
771 Asimow, P. D., Dixon, J. E., and Langmuir, C. H. (2004) A hydrous melting and fractionation
772 model for mid-ocean ridge basalts: Application to the Mid-Atlantic Ridge near the Azores.
773 Geochemistry, Geophysics, Geosystems, 5(1).
774 Balta, J. B., and McSween Jr, H. Y. (2013) Application of the MELTS algorithm to Martian
775 compositions and implications for magma crystallization. Journal of Geophysical
776 Research: Planets, 118, 2502–2519.

Always consult and cite the final, published document. See http:/www.minsocam.org or GeoscienceWorld

Bartoli, O., and Carvalho, B. B. (2021) Anatectic granites in their source region: A comparison between experiments, thermodynamic modelling and nanogranitoids. Lithos, 106046.

Bédard, J.H., 2006, A catalytic delamination-driven model for coupled genesis of Archaean crust and sub-continental lithospheric mantle. Geochimica et Cosmochimica Acta, 70, 1188–1214.

Berman, R. G. (1988) Internally-consistent thermodynamic data for minerals in the system Na_2O-K_2O-CaO-MgO-FeO-Fe_2O_3-Al_2O_3-SiO_2-TiO_2-H_2O-CO_2. Journal of Petrology, 29, 445–522.

Berman, R. G. (1990) Mixing properties of Ca-Mg-Fe-Mn garnets. American Mineralogist, 75, 328–344.

Berman, R. G. and Brown, T. H. (1985) Heat capacity of minerals in the system Na_2O–K_2O–CaO–MgO–FeO–Fe_2O_3–Al_2O_3–SiO_2–TiO_2–H_2O–CO_2: representation, estimation, and high temperature extrapolation. Contributions to Mineralogy and Petrology, 89, 168–183.

Berman, R. G., and Koziol, A. M. (1991) Ternary excess properties of grossular-pyrope-almandine garnet and their influence in geothermobarometry. American Mineralogist, 76, 1223–1231.

Berndt, J., Koepke, J., and Holtz, F. (2005) An experimental investigation of the influence of water and oxygen fugacity on differentiation of MORB at 200 MPa. Journal of Petrology, 46, 135–167.

Bohrson, W. A., Spera F. J., Heinonen, J. S., Brown, G. A., Scruggs, M. A., Adams, J. V., Takach, M., Zeff, G., and Suikkanen, E. (2020) Diagnosing open-system magmatic processes using the Magma Chamber Simulator (MCS): part I - major elements and phase equilibria. Contributions to Mineralogy and Petrology, 175, 104.

Always consult and cite the final, published document. See http:/www.minsocam.org or GeoscienceWorld

Bohrson, W. A., Spera, F. J., Ghiorso, M. S., Brown, G. A., Creamer, J. B., and Mayfield, A. (2014) Thermodynamic model for energy-constrained open-system evolution of crustal magma bodies undergoing simultaneous recharge, assimilation and crystallization: The magma chamber simulator. Journal of Petrology, 55, 1685–1717.

Bowen, N. L. (1928) The Evolution of the Igneous Rocks, Princeton, Univ. Press, Princeton, New Jersey.

Bowen, N. L. (1945) Phase equilibria bearing on the origin and differentiation of alkaline rocks. American Journal of Science, 243, 75–89.

Brown, M. (2007) Crustal melting and melt extraction, ascent and emplacement in orogens: mechanisms and consequences. Journal of the Geological Society,164, 709–730.

Carlson, R. L., and Jay Miller, D. (2004) Influence of pressure and mineralogy on seismic velocities in oceanic gabbros: Implications for the composition and state of the lower oceanic crust. Journal of Geophysical Research: Solid Earth, 109(B9), B09205.

Carmichael, I. S., Turner, F. J., and Verhoogen, J. (1974) Igneous petrology. McGraw-Hill, Inc. USA.

Connolly, J. A. (2005) Computation of phase equilibria by linear programming: a tool for geodynamic modeling and its application to subduction zone decarbonation. Earth and Planetary Science Letters, 236, 524–541.

de Capitani, C., and Brown, T. H. (1987) The computation of chemical equilibrium in complex systems containing non-ideal solutions. Geochimica et Cosmochimica Acta, 51, 2639–2652.

de Capitani, C., and Petrakakis, K. (2010) The computation of equilibrium assemblage diagrams with Theriak/Domino software. American Mineralogist, 95, 1006–1016.

Always consult and cite the final, published document. See http:/www.minsocam.org or GeoscienceWorld

This is the peer-reviewed, final accepted version for American Mineralogist, published by the Mineralogical Society of America.
The published version is subject to change. Cite as Authors (Year) Title. American Mineralogist, in press.
DOI: https://doi.org/10.2138/am-2022-8211. http://www.minsocam.org/

823 Elkins, L. T., and Grove, T. L. (1990) Ternary feldspar experiments and thermodynamic models.
824 American Mineralogist, 75, 544–559.
825 England, P. C., and Thompson, A. (1986) Some thermal and tectonic models for crustal melting
826 in continental collision zones. Geological Society, London, Special Publications, 19, 83–
827 94.
828 Essene, E. J. (1989) The current status of thermobarometry in metamorphic rocks. In: Daly, J. S.,
829 Cliff, R. A. and Yardley, B. W. D. (eds) Evolution of Metamorphic Belts. Geological
830 Society, London, Special Publications, 43, 1–44.
831 Forshaw, J. B., Waters, D. J., Pattison, D. R., Palin, R. M., and Gopon, P. (2019) A comparison
832 of observed and thermodynamically predicted phase equilibria and mineral compositions in
833 mafic granulites. Journal of Metamorphic Geology, 37, 153–179.
834 Fowler, S. J., and Spera, F. J. (2010) A metamodel for crustal magmatism: phase equilibria of
835 giant ignimbrites. Journal of Petrology, 51, 1783–1830.
836 Gale, A., Dalton, C. A., Langmuir, C. H., Su, Y., and Schilling, J. G. (2013) The mean
837 composition of ocean ridge basalts. Geochemistry, Geophysics, Geosystems, 14, 489–518.
838 García-Arias, M. (2020) Consistency of the activity–composition models of Holland, Green, and
839 Powell (2018) with experiments on natural and synthetic compositions: A comparative
840 study. Journal of Metamorphic Geology, 39, 993–1010
841 García-Arias, M., and Stevens, G. (2017) Phase equilibrium modelling of granite magma
842 petrogenesis: A. An evaluation of the magma compositions produced by crystal
843 entrainment in the source. Lithos, 277, 131–153.

Always consult and cite the final, published document. See http:/www.minsocam.org or GeoscienceWorld

844 Gervais, F., & Trapy, P. H. (2021) Testing solution models for phase equilibrium (forward)
845 modeling of partial melting experiments. Contributions to Mineralogy and Petrology, 176,
846 1–18.
847 Ghiorso, M. S. (1990) Thermodynamic properties of hematite—ilmenite—geikielite solid
848 solutions. Contributions to Mineralogy and Petrology, 104, 645–667.
849 Ghiorso, M. S., and Gualda, G. A. (2015) An H_2O–CO_2 mixed fluid saturation model compatible
850 with rhyolite-MELTS. Contributions to Mineralogy and Petrology, 169, 1–30.
851 Ghiorso, M. S., and Sack, O. (1991) Fe-Ti oxide geothermometry: thermodynamic formulation
852 and the estimation of intensive variables in silicic magmas. Contributions to Mineralogy
853 and Petrology 108, 485–510.
854 Ghiorso, M. S., and Sack, R. O. (1995) Chemical mass transfer in magmatic processes IV. A
855 revised and internally consistent thermodynamic model for the interpolation and
856 extrapolation of liquid-solid equilibria in magmatic systems at elevated temperatures and
857 pressures. Contributions to Mineralogy and Petrology, 119, 197–212.
858 Ghiorso, M. S., Evans, B. W., Hirschmann, M. M., and Yang, H. (1995) Thermodynamics of the
859 amphiboles: Fe-Mg cummingtonite solid solutions. American Mineralogist, 80, 502–519.
860 Ghiorso, M. S., Hirschmann, M. M., Reiners, P. W., and Kress, V. (2002) The pMELTS: An
861 revision of MELTS aimed at improving calculation of phase relations and major element
862 partitioning involved in partial melting of the mantle at pressures up to 3 GPa.
863 Geochemistry, Geophysics, Geosystems, 3.
864 Green, E. C. R., White, R. W., Diener, J. F. A., Powell, R., Holland, T. J. B., Palin, R. M. (2016)
865 Activity–composition relations for the calculation of partial melting equilibria in metabasic
866 rocks. Journal of Metamorphic Geology, 34, 845–869.

Always consult and cite the final, published document. See http:/www.minsocam.org or GeoscienceWorld

This is the peer-reviewed, final accepted version for American Mineralogist, published by the Mineralogical Society of America.
The published version is subject to change. Cite as Authors (Year) Title. American Mineralogist, in press.
DOI: https://doi.org/10.2138/am-2022-8211. http://www.minsocam.org/

867 Gualda, G. A., Ghiorso, M. S., Lemons, R. V., and Carley, T. L. (2012) Rhyolite-MELTS: a
868 modified calibration of MELTS optimized for silica-rich, fluid-bearing magmatic systems.
869 Journal of Petrology, 53, 875–890.
870 Guevara, V. E., and Caddick, M. J. (2016) Shooting at a moving target: Phase equilibria
871 modelling of high-temperature metamorphism. Journal of Metamorphic Geology, 34, 209–
872 235.
873 Heinonen, J. S., Luttinen, A. V., Spera, F. J., and Bohrson, W. A. (2019) Deep open storage and
874 shallow closed transport system for a continental flood basalt sequence revealed with
875 Magma Chamber Simulator. Contributions to Mineralogy and Petrology, 174, 87.
876 Hernández-Uribe, D., and Palin, R. M. (2019) A revised petrological model for subducted
877 oceanic crust: insights from phase equilibria modeling. Journal of Metamorphic Geology,
878 37, 745–768.
879 Hernández-Uribe, D., Hernández-Montenegro, J. D., Cone, K. A., and Palin, R. M. (2020)
880 Oceanic slab-top melting during subduction: Implications for trace-element recycling and
881 adakite petrogenesis. Geology, 48, 216–220.
882 Hernández-Montenegro, J. D., Palin, R. M., Zuluaga, C. A., and Hernández-Uribe, D. (2021)
883 Archean continental crust formed by magma hybridization and voluminous partial melting.
884 Scientific Reports, 11, 1–9.
885 Hirschmann, M. M., Ghiorso, M. S., Wasylenki, L. E., Asimow, P. D., and Stolper, E. M. (1998)
886 Calculation of peridotite partial melting from thermodynamic models of minerals and
887 melts. I. Review of methods and comparison with experiments. Journal of Petrology, 39,
888 1091–1115.

Always consult and cite the final, published document. See http:/www.minsocam.org or GeoscienceWorld

Holland, T. J. B., and Powell, R. (1998) An internally consistent thermodynamic data set for phases of petrological interest. Journal of Metamorphic Geology, 16, 309–343.

Holland, T. J. B., and Powell, R. (2001) Calculation of phase relations involving haplogranitic melts using an internally consistent thermodynamic dataset. Journal of Petrology, 42, 673–683.

Holland, T. J. B., and Powell, R. (2003) Activity–composition relations for phases in petrological calculations: an asymmetric multicomponent formulation. Contributions to Mineralogy and Petrology, 145, 492–501.

Holland, T. J. B., and Powell, R. (2011) An improved and extended internally consistent thermodynamic dataset for phases of petrological interest, involving a new equation of state for solids. Journal of Metamorphic Geology, 29, 333–383.

Holland, T. J., Green, E. C., and Powell, R. (2018) Melting of peridotites through to granites: a simple thermodynamic model in the system KNCFMASHTOCr. Journal of Petrology 59, 881–900.

Jennings, E. S., and Holland, T. J. (2015) A simple thermodynamic model for melting of peridotite in the system NCFMASOCr. Journal of Petrology, 56, 869–892.

Johnson, T. E., White, R. W., and Powell, R. (2008). Partial melting of metagreywacke: a calculated mineral equilibria study. Journal of Metamorphic Geology, 26, 837–853.

Johnson, T. E., Morrissey, L. J., Nemchin, A. A., Gardiner, N. J., and Snape, J. F. (2021). The phases of the Moon: Modelling crystallisation of the lunar magma ocean through equilibrium thermodynamics. Earth and Planetary Science Letters, 556, 116721.

Johnson, T. E., Brown, M., Gardiner, N. J., Kirkland, C. L., and Smithies, R. H. (2017) Earth's first stable continents did not form by subduction. Nature, 543, 239–242.

Always consult and cite the final, published document. See http:/www.minsocam.org or GeoscienceWorld

912 Kerrick, D. M. and Jacobs, G. K. (1981) A modified Redlich–Kwong equation for H_2O , CO_2,
913 and H_2O–CO_2 mixtures at elevated pressures and temperatures. American Journal of
914 Science, 281, 735–767.
915 Kerrick, D. M., and Connolly, J. A. D. (2001) Metamorphic devolatilization of subducted
916 oceanic metabasalts: implications for seismicity, arc magmatism and volatile recycling.
917 Earth and Planetary Science Letters, 189, 19–29.
918 Kendrick, J., & Yakymchuk, C. (2020) Garnet fractionation, progressive melt loss and bulk
919 composition variations in anatectic metabasites: complications for interpreting the
920 geodynamic significance of TTGs. Geoscience Frontiers, 11(3), 745–763.
921 Korhonen, F. J., Clark, C., Brown, M., and Taylor, R. J. M. (2014) Taking the temperature of
922 Earth's hottest crust. Earth and Planetary Science Letters, 408, 341–354.
923 Lanari, P., and Duesterhoeft, E. (2019) Modeling metamorphic rocks using equilibrium
924 thermodynamics and internally consistent databases: past achievements, problems and
925 perspectives. Journal of Petrology, 60, 19–56.
926 Le Bas, M. L., Maitre, R. L., Streckeisen, A., and Zanettin, B. A. (1986) A chemical
927 classification of volcanic rocks based on the total alkali-silica diagram. Journal of
928 Petrology, 27, 745–750.
929 Martin, H., Moyen, J. F., Guitreau, M., Blichert-Toft, J., and Le Pennec, J. L. (2014) Why
930 Archaean TTG cannot be generated by MORB melting in subduction zones. Lithos, 198,
931 1–13.
932 McDonough, W. F., and Sun, S. S., 1995, The composition of the Earth. Chemical Geology, 120,
933 223–253.

Always consult and cite the final, published document. See http:/www.minsocam.org or GeoscienceWorld

Moyen, J. F. (2009) High Sr/Y and La/Yb ratios: the meaning of the "adakitic signature". Lithos, 112, 556–574.

Moyen, J. F. (2011) The composite Archaean grey gneisses: petrological significance, and evidence for a non-unique tectonic setting for Archaean crustal growth. Lithos, 123, 21–36.

Moyen, J. F., and Martin, H. (2012) Forty years of TTG research. Lithos, 148, 312–336.

Palin, R.M., White, R.W. and Green, E.C.R. (2016) Partial melting of metabasic rocks and the generation of tonalitic–trondhjemitic–granodioritic (TTG) crust in the Archaean: Constraints from phase equilibrium modelling. Precambrian Research, 287, 73–90.

Palin, R. M., Reuber, G. S., White, R. W., Kaus, B. J., and Weller, O. M. (2017) Subduction metamorphism in the Himalayan ultrahigh-pressure Tso Morari massif: an integrated geodynamic and petrological modelling approach. Earth and Planetary Science Letters, 467, 108–119.

Pamukcu, A. S., Gualda, G. A., Ghiorso, M. S., Miller, C. F., and McCracken, R. G. (2015) Phase-equilibrium geobarometers for silicic rocks based on rhyolite-MELTS—Part 3: Application to the Peach Spring Tuff (Arizona–California–Nevada, USA). Contributions to Mineralogy and Petrology, 169, 33.

Pan, R., Macris, C. A., and Menold, C. A. (2020) Thermodynamic modeling of high-grade metabasites: a case study using the Tso Morari UHP eclogite. Contributions to Mineralogy and Petrology, 175, 1–28.

Pichavant, M., Weber, C., and Villaros, A. (2019) Effect of anorthite on granite phase relations: Experimental data and models. Comptes Rendus Geoscience, 351, 540–550.

Always consult and cite the final, published document. See http:/www.minsocam.org or GeoscienceWorld

Pitzer, K. S. and Sterner, S. M. (1995) Equations of state valid continuously from zero to extreme pressures with H_2O and CO_2 as examples. International Journal of Thermophysics, 16, 511–518.

Powell, R., and Holland, T. J. B. (2008) On thermobarometry. Journal of Metamorphic Geology, 26, 155–179.

Powell, R., and Holland, T. J. B. (1988) An internally consistent dataset with uncertainties and correlations: 3. Applications to geobarometry, worked examples and a computer program. Journal of metamorphic Geology, 6, 173–204.

Powell, R., Guiraud, M., and White, R. W. (2005) Truth and beauty in metamorphic phase-equilibria: conjugate variables and phase diagrams. The Canadian Mineralogist, 43, 21–33.

Powell, R., Holland, T. J. B., and Worley, B. A. (1998) Calculating phase diagrams involving solid solutions via non-linear equations, with examples using THERMOCALC. Journal of metamorphic Geology, 16, 577–588.

Robie, R. A., Hemingway, B. S. and Fisher, J. R. (1978) Thermodynamic properties of minerals and related substances at 298.15K and 1 bar (105 pascals) pressure and at higher temperatures. US Geological Survey Bulletin, 1452, 456 pp.

Sack, R. O., and Ghiorso, M. S. (1989) Importance of considerations of mixing properties in establishing an internally consistent thermodynamic database: thermochemistry of minerals in the system Mg_2SiO_4–Fe_2SiO_4–SiO_2. Contributions to Mineralogy and Petrology, 102, 41–68.

Sack, R. O., and Ghiorso, M. S. (1991a) An internally consistent model for the thermodynamic properties of Fe− Mg-titanomagnetite-aluminate spinels. Contributions to Mineralogy and Petrology, 106, 474–505.

Always consult and cite the final, published document. See http:/www.minsocam.org or GeoscienceWorld

978 Sack, R. O., and Ghiorso, M. S. (1991b) Chromian spinels as petrogenetic indicators:
979 Thermodynamics and petrological applications. American Mineralogist, 76(5–6), 827–847.
980 Sack, R. O., and Ghiorso, M. S. (1994) Thermodynamics of multicomponent pyroxenes: I.
981 Formulation of a general model. Contributions to Mineralogy and Petrology, 116(3), 277–
982 286.
983 Santos, C. A., Moraes, R., and Szabó, G. A. (2019) A comparison between phase diagram
984 modelling of metamafic rocks and experimental and independent thermobarometric data.
985 Lithos, 340, 108–123.
986 Sen, C., and Dunn, T. (1994) Dehydration melting of a basaltic composition amphibolite at 1.5
987 and 2.0 GPa: implications for the origin of adakites. Contributions to Mineralogy and
988 Petrology, 117(4), 394–409.
989 Shaw, D.M., 2006, Trace elements in magmas: a theoretical treatment. Cambridge University
990 Press.
991 Spera, F. J., Bohrson, W. A., Till, C. B., and Ghiorso, M. S. (2007) Partitioning of trace elements
992 among coexisting crystals, melt, and supercritical fluid during isobaric crystallization and
993 melting. American Mineralogist, 92, 1881–1898.
994 Starr, P. G., Pattison, D. R., and Ames, D. E. (2020) Mineral assemblages and phase equilibria of
995 metabasites from the prehnite–pumpellyite to amphibolite facies, with the Flin Flon
996 Greenstone Belt (Manitoba) as a type example. Journal of Metamorphic Geology, 38, 71-
997 102.
998 Stuck, T. J., & Diener, J. F. (2018) Mineral equilibria constraints on open-system melting in
999 metamafic compositions. Journal of Metamorphic Geology, 36, 255–281.

Always consult and cite the final, published document. See http:/www.minsocam.org or GeoscienceWorld

Sun, S. S., and McDonough, W. F. (1989) Chemical and isotopic systematics of oceanic basalts: implications for mantle composition and processes. Geological Society, London, Special Publications, 42, 313–345.

Thompson, J. B. (1967) Thermodynamic properties of simple solutions: in Abelson, P.H., ed., Researches in Geochemistry, Vol. 2, John Wiley and Sons, mmInc., New York.

Tomlinson, E. L., and Holland, T. J. (2021) A thermodynamic model for the subsolidus evolution and melting of peridotite. Journal of Petrology, 62, egab012.

Turcotte, D. L., and Schubert, G. (2002) Geodynamics. Cambridge university press. UK

White, R. W., Powell, R., and Holland, T. J. B. (2001) Calculation of partial melting equilibria in the system Na_2O–CaO–K_2O–FeO–MgO–Al_2O_3–SiO_2–H_2O (NCKFMASH) Journal of metamorphic Geology, 19, 139–153.

White, R. W., Powell, R., and Holland, T. J. B. (2007) Progress relating to calculation of partial melting equilibria for metapelites. Journal of Metamorphic Geology, 25, 511–527.

White, R. W., Powell, R., Holland, T. J. B. and Worley, B. A. (2000) The effect of TiO_2 and Fe_2O_3 on metapelitic assemblages at greenschist and amphibolite facies conditions: mineral equilibria calculations in the system K_2O–FeO–MgO–Al_2O_3–SiO_2–H_2O–TiO_2–Fe_2O_3. Journal of Metamorphic Geology, 18, 497–511.

White, R. W., Powell, R., Holland, T. J. B., Johnson, T. E., and Green, E. C. R. (2014) New mineral activity–composition relations for thermodynamic calculations in metapelitic systems. Journal of Metamorphic Geology, 32, 261–286.

White, R. W., and Powell, R. (2002) Melt loss and the preservation of granulite facies mineral assemblages. Journal of Metamorphic Geology, 20, 621–632.

Always consult and cite the final, published document. See http:/www.minsocam.org or GeoscienceWorld

White, R. W., Stevens, G., and Johnson, T. E. (2011) Is the crucible reproducible? Reconciling melting experiments with thermodynamic calculations. Elements, 7, 241–246.

Whitney, D. L., and Evans, B. W. (2010) Abbreviations for names of rock–forming minerals. American Mineralogist, 95, 185–187.

Whittington, A., Hofmeister, A. and Nabelek, P. (2009) Temperature-dependent thermal diffusivity of the Earth's crust and implications for magmatism. Nature, 458, 319–321

Yakymchuk, C. (2017) Applying phase equilibria modelling to metamorphic and geological processes: recent developments and future potential. Geoscience Canada, 44, 27–45.

Yakymchuk, C., and Brown, M. (2014) Consequences of open-system melting in tectonics. Journal of the Geological Society, 171, 21–40.

FIGURE CAPTIONS

Figure 1. Equilibrium phase assemblages at 0.25 GPa for a N-MORB composition. (a, b) rhyolite-MELTS and (c, d) HPx-mb16. (a, c) Low-H_2O (0.5 wt% H_2O) calculations. (b, d) High-H_2O (4 wt% H_2O) calculations. Mineral abbreviations follow Whitney and Evans (2010) with the exception of "L" and "F" which refer to liquid and fluid, respectively.

Figure 2. Equilibrium phase assemblages at 1 GPa for a N-MORB composition. (a, b) rhyolite-MELTS and (c, d) HPx-mb16. (a, c) Low-H_2O (0.5 wt% H_2O) calculations. (b, d) High-H_2O (4 wt% H_2O) calculations. Mineral abbreviations follow Whitney and Evans (2010) with the exception of "L" and "F" which refer to liquid and fluid, respectively.

Figure 3. Total alkali-silica (TAS) classification diagram (Le Bas et al*.,* 1986) for the calculated N-MORB liquids (liquid compositions correspond to those presented in Figs.. 1 and 2). Liquid compositions are shown every 10 °C from the liquidus to the solidus.

Always consult and cite the final, published document. See http:/www.minsocam.org or GeoscienceWorld

Figure 4. Liquid compositional evolution (wt%) at 0.25 GPa for a low-H_2O (0.5 wt H_2O) N-MORB composition. (a–f) Calculated liquid compositions as a function of temperature. (g–i) Liquid compositions shown in Harker diagrams. Approximate liquid fractions (wt%) are shown in (a) for comparison between modeling approaches. Mineral abbreviations follow Whitney and Evans (2010) with the exception of "L" and "F" which refer to liquid and fluid, respectively.

Figure 5. Liquid compositional evolution (wt%) at 0.25 GPa for a high-H_2O (4 wt H_2O) N-MORB composition. (a–f) Modeled liquid compositions as a function of temperature. (g–i) Modeled liquid compositions shown in Harker diagrams. Approximate liquid fractions (wt%) are shown in (a) for comparison between modeling approaches. Mineral abbreviations follow Whitney and Evans (2010) with the exception of "L" and "F" which refer to liquid and fluid, respectively.

Figure 6. Liquid compositional evolution (wt%) at 1 GPa for a low-H_2O (0.5 wt H_2O) N-MORB composition. (a–f) Modeled liquid compositions as a function of temperature. (g–i) Modeled liquid compositions shown in Harker diagrams. Approximate liquid fractions (wt%) are shown in (a) for comparison between modeling approaches. Mineral abbreviations follow Whitney and Evans (2010) with the exception of "L" and "F" which refer to liquid and fluid, respectively.

Figure 7. Liquid compositional evolution (wt%) at 1 GPa for a high-H_2O (4 wt H_2O) N-MORB composition. (a–f) Modeled liquid compositions as a function of temperature. (g–i) Modeled liquid compositions shown in Harker diagrams. Approximate liquid fractions (in wt%) are shown in (a) for comparison between modeling approaches. Mineral abbreviations follow Whitney and Evans (2010) with the exception of "L" and "F" which refer to liquid and fluid, respectively.

Figure 8. Liquid incompatible trace-element patterns at (a–b) 900 °C in the low-*P*–low-H_2O run, (c–d) 1000 °C in the high-*P*–low-H_2O run, and (e–f) 850 °C in the high-*P*–high-H_2O run. (a), (c),

Always consult and cite the final, published document. See http:/www.minsocam.org or GeoscienceWorld

and (e) normalized to primitive mantle (Sun and McDonough, 1989) and (b), (d), and (f) normalized to chondrite (McDonough and Sun, 1995). The orange line is mean N-MORB from Gale et al. (2013).

Figure 9. Phase proportion comparison experiments of basaltic compositions and model predictions. (a, b) Comparison with Berndt et al. (2005) experiments (BKH). (c, d) Comparison with Sen and Dunn, 1994 (SD). Phase proportions are shown on an anhydrous basis (recalcualted to 100%). In the SD experiments, rutile is also present as a trace phase. Rhyolite-MELTS models where calculated with rhyolite-MELTS v1.2.0. Mineral abbreviations follow Whitney and Evans (2010) with the exception of "L" and "F" which refer to liquid and fluid, respectively.

TABLE CAPTIONS

Table 1. Bulk-rock compositions used for petrological modeling (normalized wt%).

Table 2. Phase proportions of N-MORB at 0.25 and 1 GPa (wt%).

Table 3. Liquid trace-element compositions (ppm).

Table 4. Comparison of phase proportions between experiments of basaltic compositions and model predictions (wt%).

Table 5. Comparison of liquid compositions between experiments of basaltic compositions and model predictions (wt%).

SUPPLEMENTARY MATERIAL

Appendix 1. The Appendix 1 describes the phase evolution as well as the liquid and mineral composition evolution. The appendix also include the mineral composition comparison between

Always consult and cite the final, published document. See http:/www.minsocam.org or GeoscienceWorld

rhyolite-MELTS and HPx-mb16, Supplementary Tables S1–S4, and Supplementary Figures S1–S6.

Figure S1. Equilibrium phase assemblages at 0.25 GPa for a N-MORB composition in vol%. (a, b) rhyolite-MELTS and (c, d) HPx-mb16. (a, c) Low-H_2O (0.5 wt% H_2O) calculations. (b, d) High-H_2O (4 wt% H_2O) calculations. Mineral abbreviations follow Whitney and Evans (2010) with the exception of "L" and "F" which refer to liquid and fluid, respectively.

Figure S2. Equilibrium phase assemblages at 1 GPa for a N-MORB composition in vol%. (a, b) rhyolite-MELTS and (c, d) HPx-mb16. (a, c) Low-H_2O (0.5 wt% H_2O) calculations. (b, d) High-H_2O (4 wt% H_2O) calculations. Mineral abbreviations follow Whitney and Evans (2010) with the exception of "L" and "F" which refer to liquid and fluid, respectively.

Figure S3. Calculated clinopyroxene compositions (in atoms per formula unit, a.p.f.u.) at (a–f) 0.25 GPa and (g–l) 1 GPa. (a–c and g–i) Clinopyroxene compositions in a low-H_2O (0.5 wt%) MORB composition. (d–f and j–l) Clinopyroxene compositions in a high-H_2O (4 wt%)MORB composition. Mineral abbreviations are the same as in Figure 1.

Figure S4. Calculated anorthite content (An) in plagioclase. (a) Plagioclase compositions at 0.25 GPa for a low-H_2O (0.5 wt%) MORB composition. (b) Plagioclase compositions at 0.25 GPa for a high-H_2O (4 wt%) MORB composition. (c) Plagioclase compositions at 1 GPa for a low-H_2O (0.5 wt%) MORB composition. Mineral abbreviations are the same as in Figure 1.

Figure S5. Calculated orthopyroxene compositions (in atoms per formula unit, a.p.f.u.) at 0.25 GPa for a low-H_2O (0.5 wt%) MORB composition.

Figure S6. Calculated garnet compositional evolution (in end-member proportions) at 1 GPa for a low-H_2O (0.5 wt%) MORB composition.

Always consult and cite the final, published document. See http:/www.minsocam.org or GeoscienceWorld

This is the peer-reviewed, final accepted version for American Mineralogist, published by the Mineralogical Society of America.
The published version is subject to change. Cite as Authors (Year) Title. American Mineralogist, in press.
DOI: https://doi.org/10.2138/am-2022-8211. http://www.minsocam.org/

1112 **Table S1.** Components considered in the activity–composition relations used in this work (see

1113 text for detail).

1114 **Table S2.** Liquid compositions of N-MORB at 0.25 GPa (wt%).

1115 **Table S3.** Liquid compositions of N-MORB at 1 GPa (wt%).

1116 **Table S4.** Amphibole composition comparison at 1 GPa (wt%).

1117 **Table S5.** Phase proportions used for trace-element modeling (wt%).

1118 **Table S6.** Partition coefficients from Bedard (2006).

Always consult and cite the final, published document. See http:/www.minsocam.org or GeoscienceWorld

This is the peer-reviewed, final accepted version for American Mineralogist, published by the Mineralogical Society of America.
The published version is subject to change. Cite as Authors (Year) Title. American Mineralogist, in press.
DOI: https://doi.org/10.2138/am-2022-8211. http://www.minsocam.org/

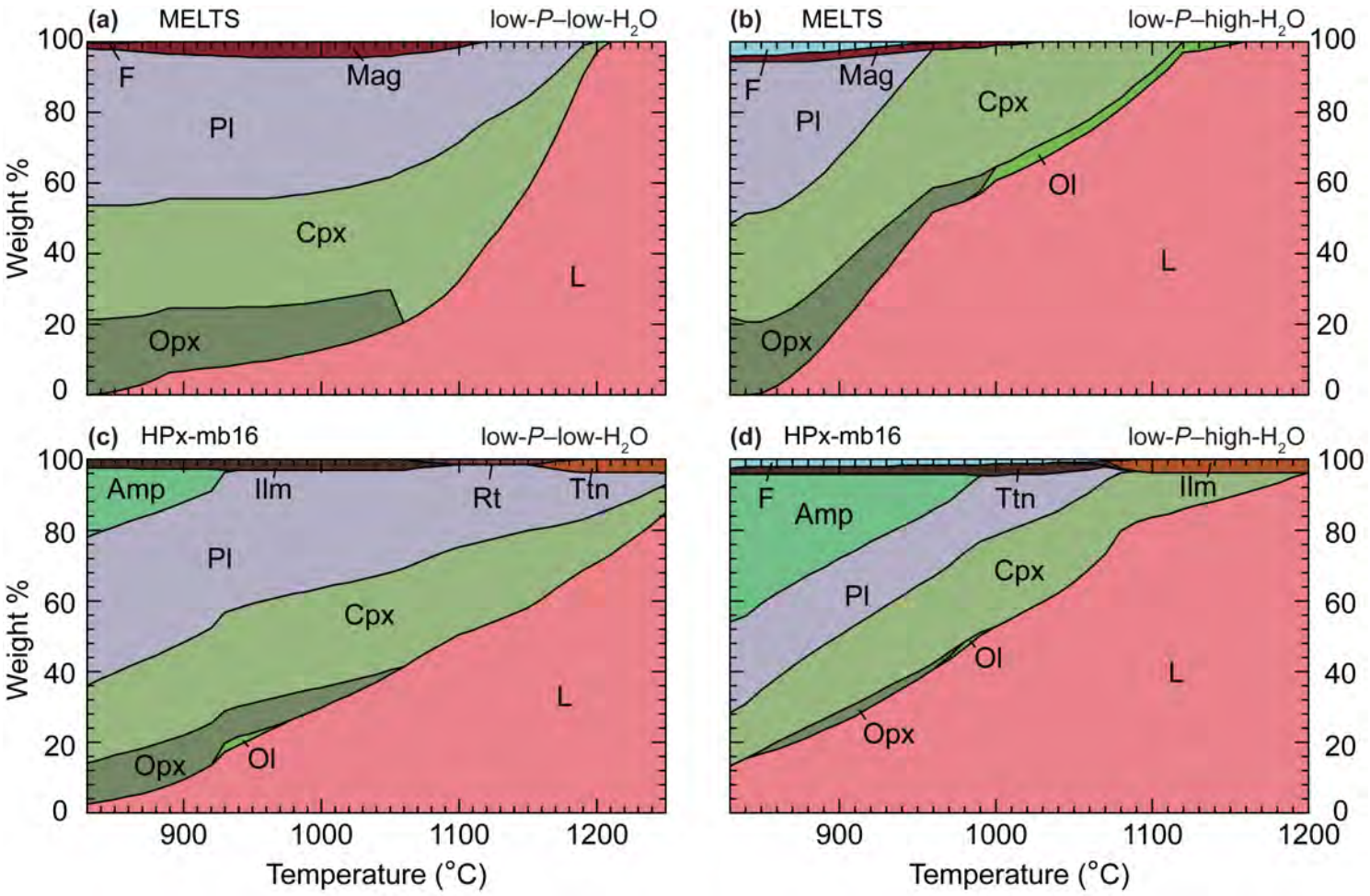

Figure 1

Always consult and cite the final, published document. See http:/www.minsocam.org or GeoscienceWorld

This is the peer-reviewed, final accepted version for American Mineralogist, published by the Mineralogical Society of America.
The published version is subject to change. Cite as Authors (Year) Title. American Mineralogist, in press.
DOI: https://doi.org/10.2138/am-2022-8211. http://www.minsocam.org/

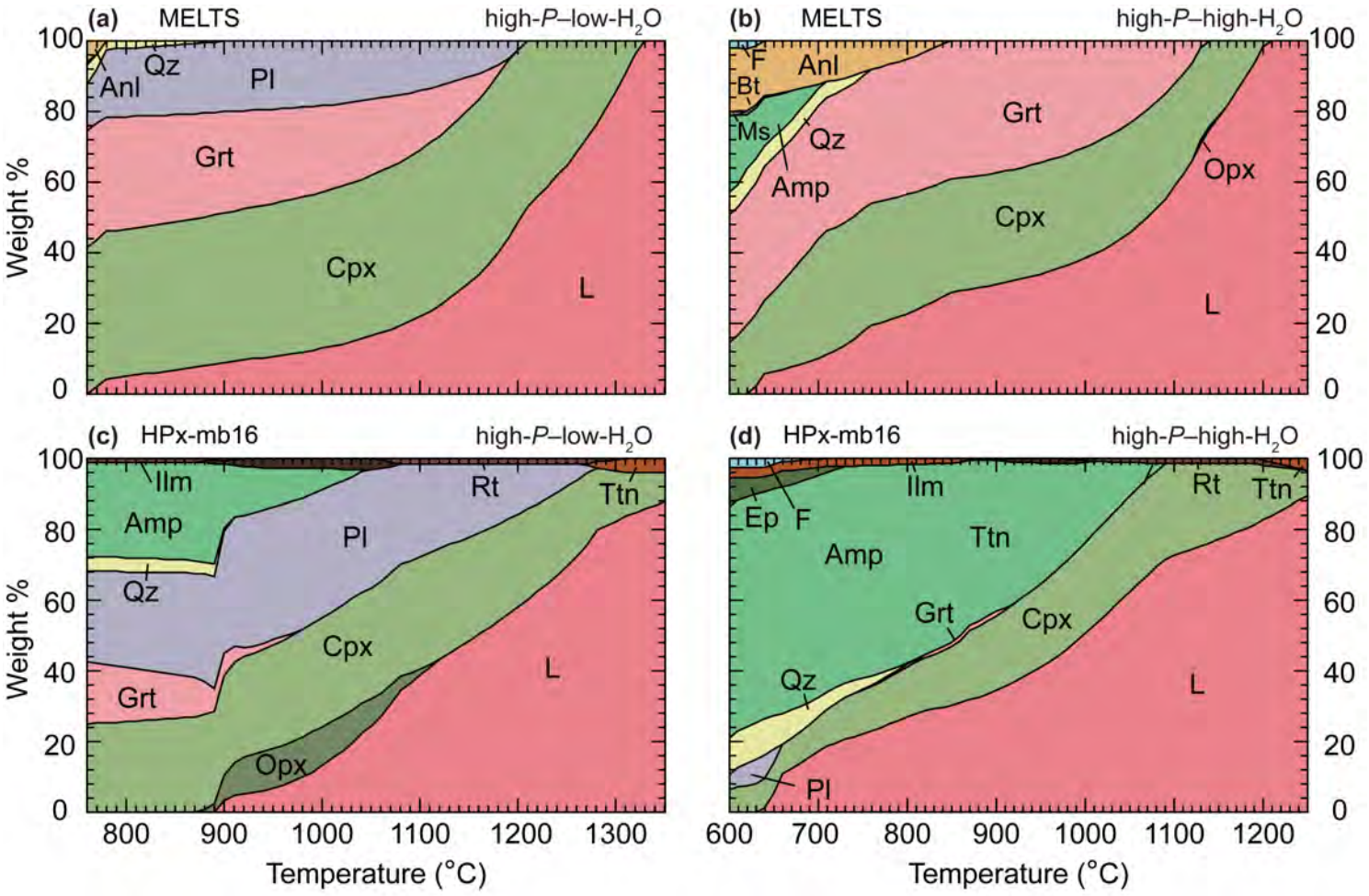

Figure 2

Always consult and cite the final, published document. See http:/www.minsocam.org or GeoscienceWorld

This is the peer-reviewed, final accepted version for American Mineralogist, published by the Mineralogical Society of America.
The published version is subject to change. Cite as Authors (Year) Title. American Mineralogist, in press.
DOI: https://doi.org/10.2138/am-2022-8211. http://www.minsocam.org/

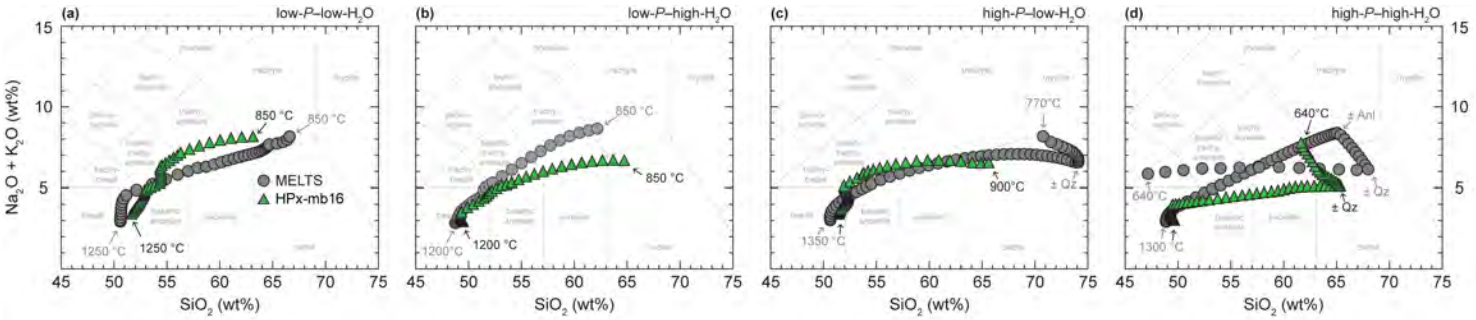

Figure 3

Always consult and cite the final, published document. See http:/www.minsocam.org or GeoscienceWorld

This is the peer-reviewed, final accepted version for American Mineralogist, published by the Mineralogical Society of America.
The published version is subject to change. Cite as Authors (Year) Title. American Mineralogist, in press.
DOI: https://doi.org/10.2138/am-2022-8211. http://www.minsocam.org/

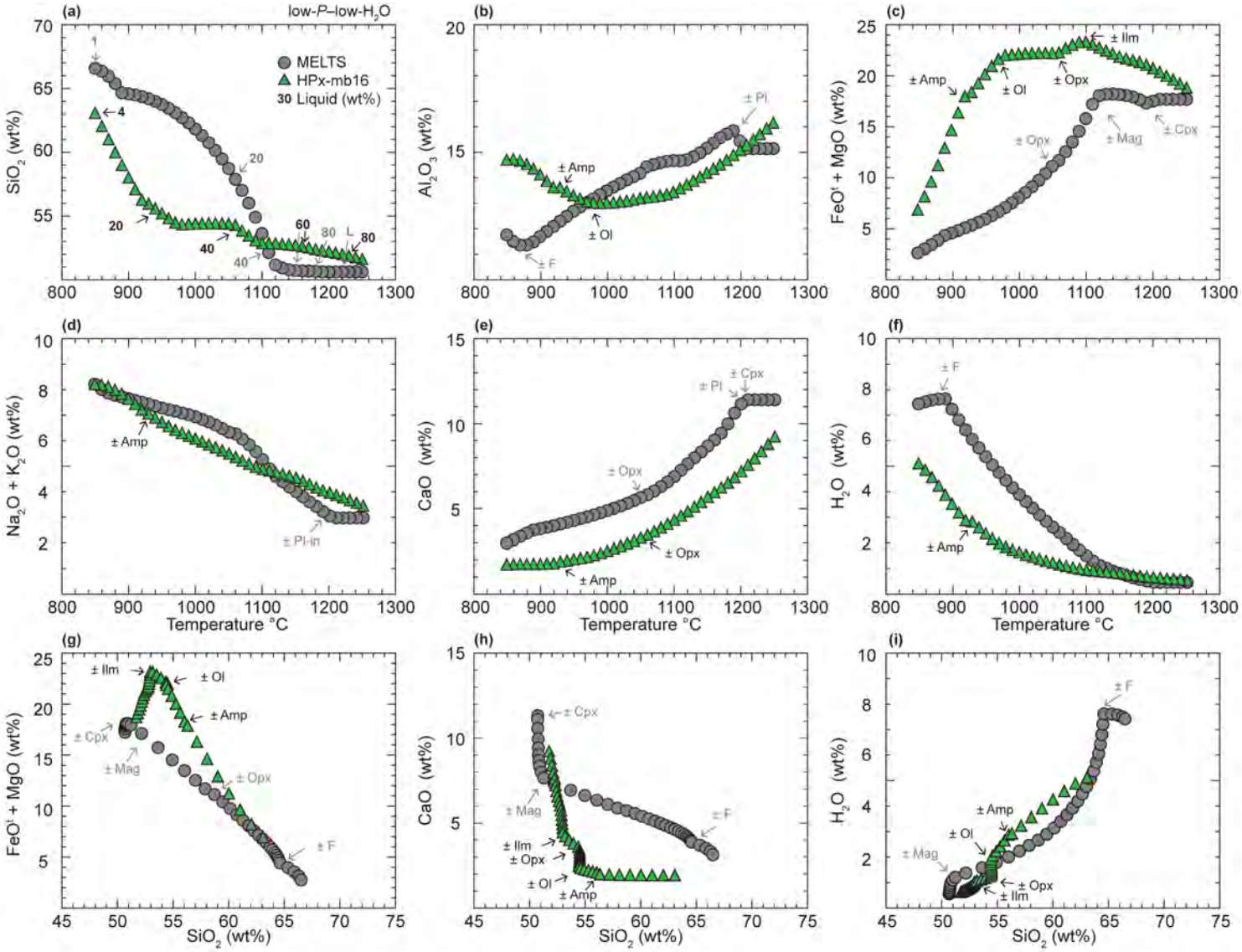

Figure 4

Always consult and cite the final, published document. See http:/www.minsocam.org or GeoscienceWorld

This is the peer-reviewed, final accepted version for American Mineralogist, published by the Mineralogical Society of America.
The published version is subject to change. Cite as Authors (Year) Title. American Mineralogist, in press.
DOI: https://doi.org/10.2138/am-2022-8211. http://www.minsocam.org/

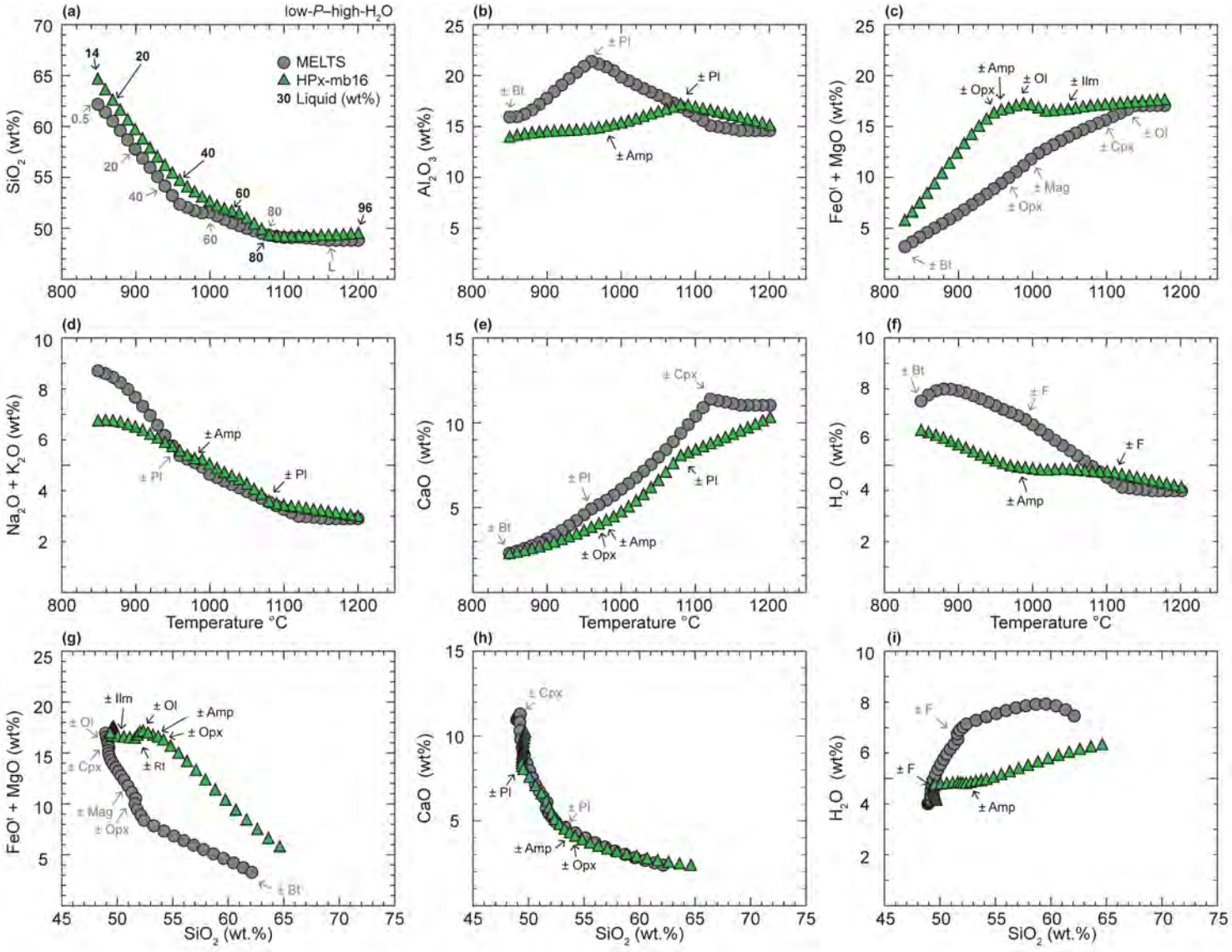

Figure 5

Always consult and cite the final, published document. See http:/www.minsocam.org or GeoscienceWorld

This is the peer-reviewed, final accepted version for American Mineralogist, published by the Mineralogical Society of America.
The published version is subject to change. Cite as Authors (Year) Title. American Mineralogist, in press.
DOI: https://doi.org/10.2138/am-2022-8211. http://www.minsocam.org/

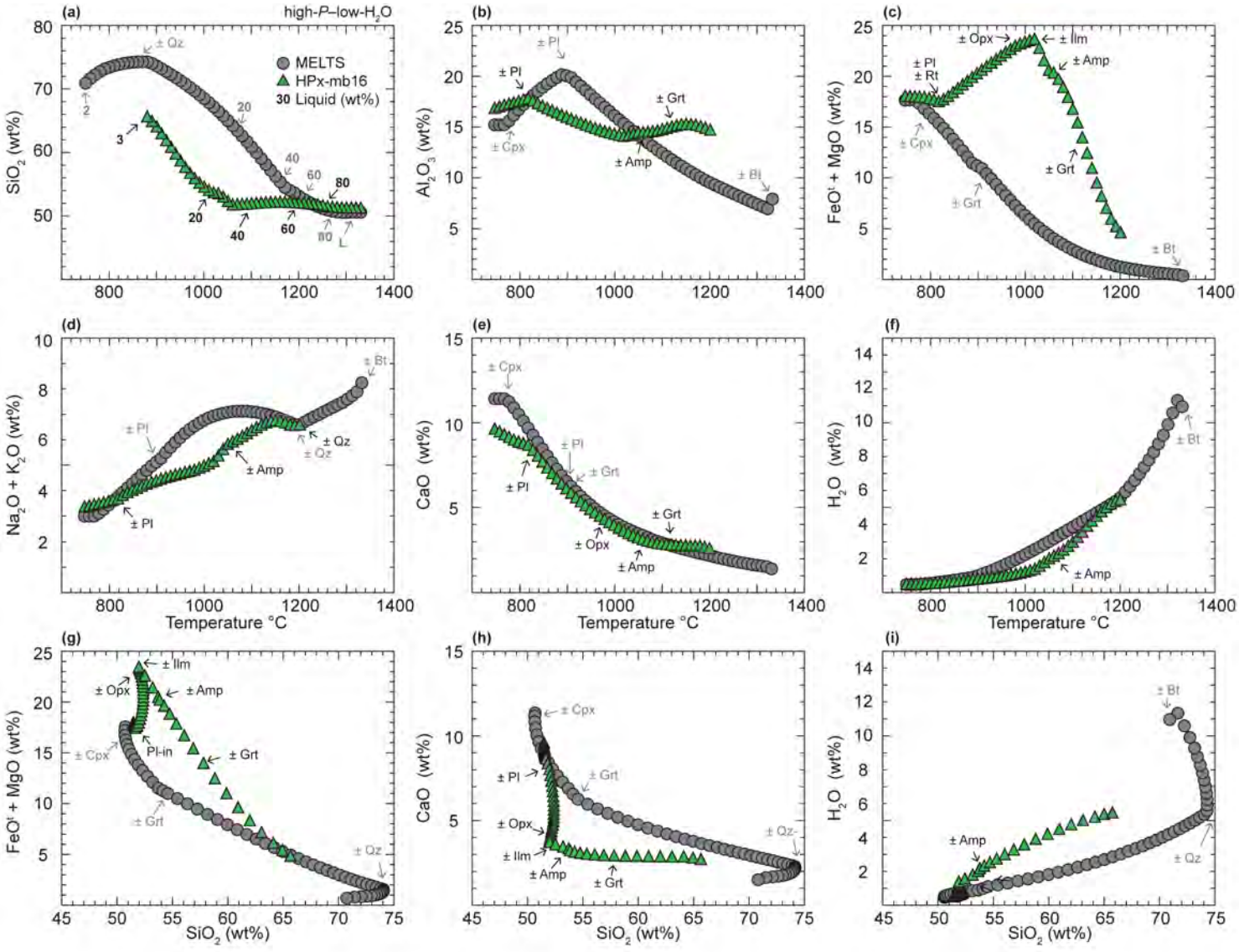

Figure 6

Always consult and cite the final, published document. See http:/www.minsocam.org or GeoscienceWorld

This is the peer-reviewed, final accepted version for American Mineralogist, published by the Mineralogical Society of America.
The published version is subject to change. Cite as Authors (Year) Title. American Mineralogist, in press.
DOI: https://doi.org/10.2138/am-2022-8211. http://www.minsocam.org/

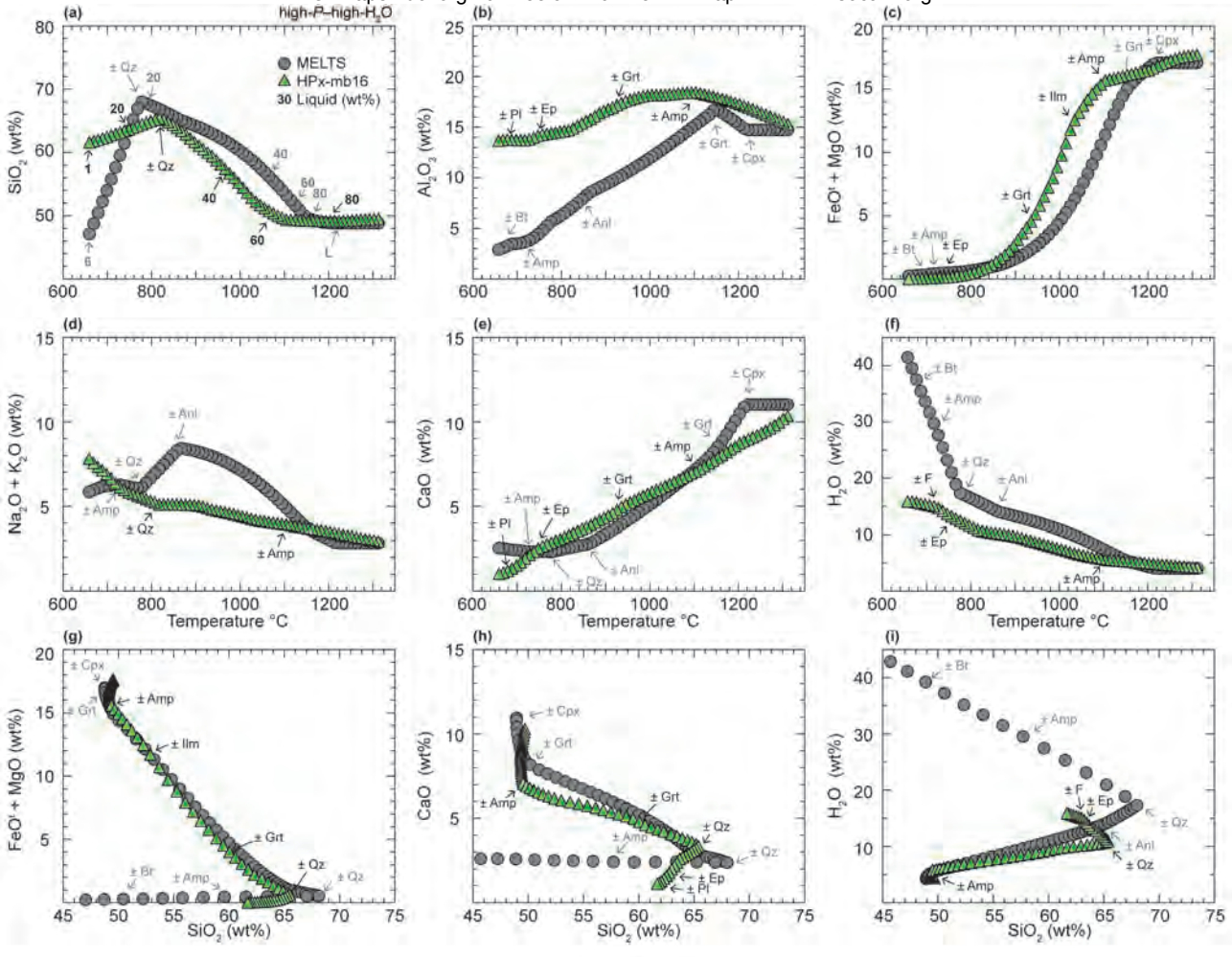

Figure 7

Always consult and cite the final, published document. See http:/www.minsocam.org or GeoscienceWorld

This is the peer-reviewed, final accepted version for American Mineralogist, published by the Mineralogical Society of America.
The published version is subject to change. Cite as Authors (Year) Title. American Mineralogist, in press.
DOI: https://doi.org/10.2138/am-2022-8211. http://www.minsocam.org/

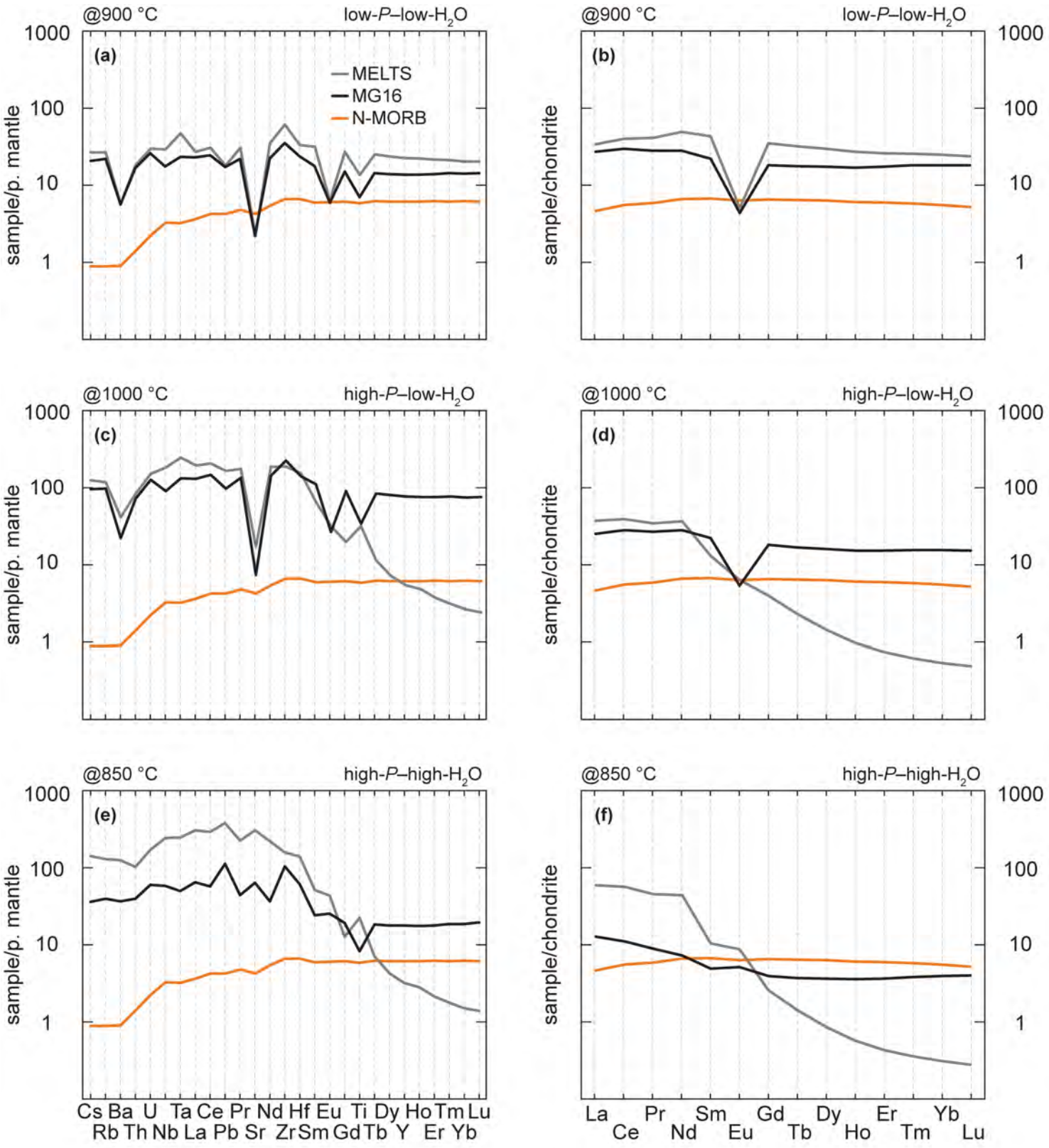

Figure 8

Always consult and cite the final, published document. See http:/www.minsocam.org or GeoscienceWorld

This is the peer-reviewed, final accepted version for American Mineralogist, published by the Mineralogical Society of America.
The published version is subject to change. Cite as Authors (Year) Title. American Mineralogist, in press.
DOI: https://doi.org/10.2138/am-2022-8211. http://www.minsocam.org/

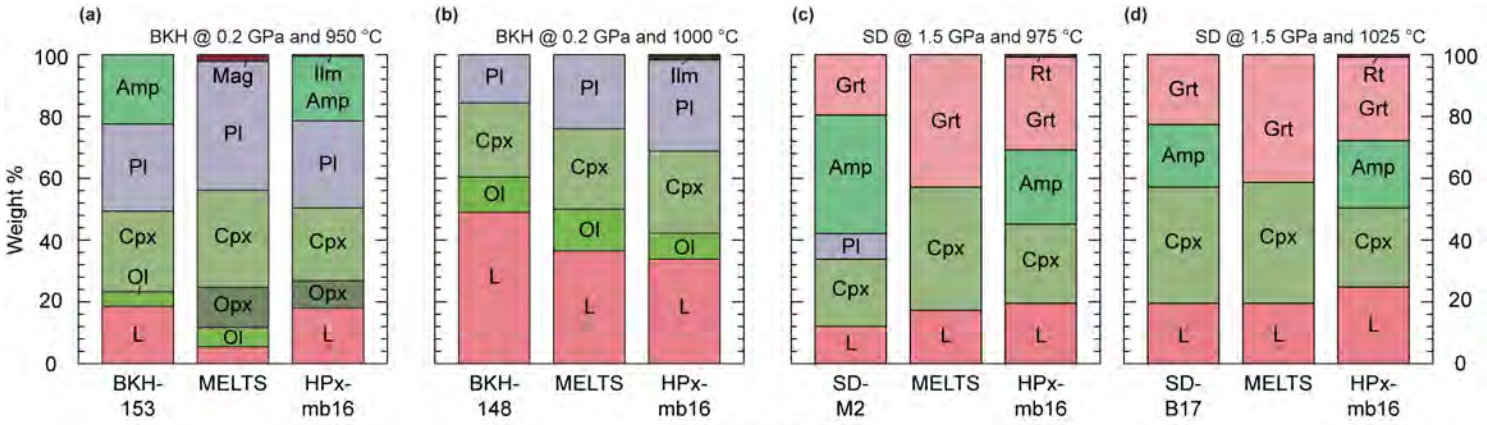

Figure 9

Always consult and cite the final, published document. See http:/www.minsocam.org or GeoscienceWorld

This is the peer-reviewed, final accepted version for American Mineralogist, published by the Mineralogical Society of America.
The published version is subject to change. Cite as Authors (Year) Title. American Mineralogist, in press.
DOI: https://doi.org/10.2138/am-2022-8211. http://www.minsocam.org/

Table 1. Bulk-rock compositions used for petrological modelling (normalized wt%).

	N-MORB–0.5	N-MORB–4
SiO_2	50.69	48.91
TiO_2	1.54	1.48
Al_2O_3	15.21	14.68
FeO^t	9.86	9.52
MgO	7.80	7.53
CaO	11.41	11.01
Na_2O	2.85	2.75
K_2O	0.14	0.14
H_2O	0.50	4.00
Total	100.00	100.00

All compositions correspond to the mean N-MORB from Gale et al. (2013) but with different H_2O contents.

Always consult and cite the final, published document. See http:/www.minsocam.org or GeoscienceWorld

This is the peer-reviewed, final accepted version for American Mineralogist, published by the Mineralogical Society of America.
The published version is subject to change. Cite as Authors (Year) Title. American Mineralogist, in press.
DOI: https://doi.org/10.2138/am-2022-8211. http://www.minsocam.org/

Table 2. Phase proportions of N-MORB at 0.25 and 1 GPa (wt%).

	L	Ol	Opx	Cpx	Grt	Fsp	Qz	Amp	Anl	Ilm	Mag	Ttn	Rt	F	Total	Solids	Fluid	Melt	Total
0.25 Gpa																			
0.5 wt% H_2O																			
900 °C																			
MELTS	7	–	18	31	–	41	–	–	–	–	4	–	–	–	100	93	–	7	100
HPx-mb16	9	–	13	26	–	40	–	9	–	3	–	–	–	–	100	91	–	9	100
1000 °C																			
MELTS	13	–	14	31	–	38	–	–	–	–	5	–	–	–	100	87	–	13	100
HPx-mb16	30	–	6	28	–	33	–	–	–	3	–	–	–	–	100	70	–	30	100
1100 °C																			
MELTS	32	–	–	39	–	27	–	–	–	–	2	–	–	–	100	68	–	32	100
HPx-mb16	50	–	–	25	–	23	–	–	–	–	–	–	2	–	100	50	–	50	100
4 wt% H_2O																			
900 °C																			
MELTS	19	–	17	32	–	27	–	–	–	–	2	–	–	2	100	78	2	19	100
HPx-mb16	26	–	3	21	–	22	–	24	–	2	–	–	–	2	100	72	2	26	100
1000 °C																			
MELTS	61	4	–	34	–	–	–	–	–	–	1	–	–	–	100	39	–	61	100
HPx-mb16	52	1	–	25	–	17	–	–	–	3	–	–	–	1	100	46	1	52	100
1100 °C																			
MELTS	88	3	–	8	–	–	–	–	–	–	–	–	–	–	100	12	–	88	100
HPx-mb16	84	–	–	13	–	–	–	–	–	–	–	–	4	<1	100	16	<1	84	100
1 Gpa																			
0.5 wt% H_2O																			
800 °C																			
MELTS	5	–	–	42	32	19	2	–	–	–	–	–	–	–	100	95	–	5	100
HPx-mb16	0	–	–	26	15	27	4	27	–	–	–	–	1	–	100	100	–	0	100
900 °C																			
MELTS	9	–	–	42	29	20	<1	–	–	–	–	–	–	–	100	91	–	9	100
HPx-mb16	3	–	7	28	7	35	1	18	–	1	–	–	1	–	100	97	–	3	100
1000 °C																			
MELTS	13	–	–	44	25	18	–	–	–	–	–	–	–	–	100	87	–	13	100
HPx-mb16	13	–	11	31	–	36	–	6	–	3	–	–	–	–	100	87	–	13	100
1100 °C																			
MELTS	22	–	–	47	17	14	–	–	–	–	–	–	–	–	100	78	–	22	100
HPx-mb16	39	–	2	32	–	26	–	–	–	–	–	–	2	–	100	61	–	39	100
4 wt% H_2O																			
800 °C																			
MELTS	23	–	–	34	38	–	–	–	5	–	–	–	–	–	100	77	–	23	100
HPx-mb16	27	–	–	14	–	1	<1	56	–	–	–	–	2	–	100	73	–	27	100
900 °C																			
MELTS	31	–	–	32	37	–	–	–	–	–	–	–	–	–	100	69	–	31	100
HPx-mb16	34	–	–	21	1	–	–	43	–	<1	–	1	–	–	100	66	–	34	100
1000 °C																			
MELTS	38	–	–	32	30	–	–	–	–	–	–	–	–	–	100	62	–	38	100
HPx-mb16	50	–	–	26	–	–	–	23	–	1	–	1	–	–	100	50	–	50	100
1100 °C																			
MELTS	59	–	–	29	12	–	–	–	–	–	–	–	–	–	100	41	–	59	100
HPx-mb16	73	–	–	26	–	–	–	–	–	–	–	1	–	–	100	27	–	73	100

Mineral abbreviations follow Whitney & Evans (2010) with the exception of “L” and "F" which refer to liquid and fluid, respectively.

Always consult and cite the final, published document. See http:/www.minsocam.org or GeoscienceWorld

This is the peer-reviewed, final accepted version for American Mineralogist, published by the Mineralogical Society of America.
The published version is subject to change. Cite as Authors (Year) Title. American Mineralogist, in press.
DOI: https://doi.org/10.2138/am-2022-8211. http://www.minsocam.org/

Table 3. Liquid trace-element compositions (ppm).

Always consult and cite the final, published document. See http:/www.minsocam.org or GeoscienceWorld

This is the peer-reviewed, final accepted version for American Mineralogist, published by the Mineralogical Society of America.
The published version is subject to change. Cite as Authors (Year) Title. American Mineralogist, in press.
DOI: https://doi.org/10.2138/am-2022-8211. http://www.minsocam.org/

Table 4. Comparison of phase proportions between experiments of basaltic compositions and model predictions (wt%).

	0.2 GPa and 950 °C					0.2 GPa and 1000 °C					1.5 GPa and 975 °C				
	BKH (153)	MELTS	HPx-mb16	% diff.[1]	% diff.[2]	BKH (148)	MELTS	HPx-mb16	% diff.[1]	% diff.[2]	SD (M2)	MELTS	HPx-mb16	% diff.[1]	% diff.[2]
L	19	6	18	*-70*	*-3*	49	37	33	*-25*	*-31*	12	17	20	*40*	*61*
Ol	5	6	–	*29*	–	11	14	9	*19*	*-24*	–	–	–	–	–
Opx	–	13	9	–	–	–	–	–	–	–	–	–	–	–	–
Cpx	26	31	24	*21*	*-9*	24	26	27	*8*	*10*	21	40	26	*89*	*21*
Pl	29	42	28	*47*	*-1*	16	24	30	*53*	*90*	9	–	–	–	–
Amp	22	–	21	–	*-8*	–	–	–	–	–	39	–	24	–	*-39*
Ilm	–	–	<1	–	–	–	–	2	–	–	–	–	–	–	–
Mag	–	2	–	–	–	–	–	–	–	–	–	–	–	–	–
Grt	–	–	–	–	–	–	–	–	–	–	19	43	30	*122*	*58*
Rt	–	–	–	–	–	–	–	–	–	–	tr	–	<1	–	–

[1]difference between the experiment and MELTS; [2]difference between the experiment and HPx-mb16. tr–trace; BKH–Berndt et al. (2005); SD–Sen & Dunn (1994). Mineral abbre
of "L" which refers to liquid. Phase proportions are shown in an anhydrous basis (recalcualted to 100%).

Always consult and cite the final, published document. See http:/www.minsocam.org or GeoscienceWorld

This is the peer-reviewed, final accepted version for American Mineralogist, published by the Mineralogical Society of America.
The published version is subject to change. Cite as Authors (Year) Title. American Mineralogist, in press.
DOI: https://doi.org/10.2138/am-2022-8211. http://www.minsocam.org/

Table 5. Comparison of liquid compositions between experiments of basaltic compositions and model predictions (wt%).

	0.2 GPa and 950 °C					0.2 GPa and 1000 °C					1.5 GPa and 925 °C				
	BKH (153)	MELTS	HPx-mb1	% diff.[1]	% diff.[2]	BKH (148)	MELTS	HPx-mb1	% diff.[1]	% diff.[2]	SD (M2)	MELTS	HPx-mb1	% diff.[1]	% diff.[2]
L fraction (wt. %)	19	6	18	*-70*	*-3*	49	37	33	*-25*	*-31*	12	17	20	*40*	*61*
SiO_2	55.77	59.67	55.60	*7*	*0*	50.83	54.83	53.90	*8*	*6*	65.29	67.33	63.18	*3*	*-3*
TiO_2	1.13	0.30	–	*-74*	–	1.19	0.52	–	*-56*	–	0.76	0.39	–	*-49*	–
Al_2O_3	16.78	14.10	14.48	*-16*	*-14*	18.37	15.73	15.00	*-14*	*-18*	18.53	12.25	18.16	*-34*	*-2*
FeO^t	8.56	4.89	10.96	*-43*	*28*	8.16	7.46	10.85	*-9*	*33*	2.85	2.02	4.93	*-29*	*73*
MgO	2.40	2.28	5.16	*-5*	*115*	3.61	3.70	6.29	*3*	*74*	0.72	0.54	1.21	*-25*	*68*
CaO	6.30	4.72	3.19	*-25*	*-49*	9.10	7.36	4.28	*-19*	*-53*	2.63	2.13	3.11	*-19*	*18*
Na_2O	3.96	6.62	5.80	*67*	*46*	3.75	4.48	5.22	*19*	*39*	6.49	10.26	5.81	*58*	*-10*
K_2O	0.22	1.06	0.38	*382*	*74*	0.15	0.21	0.23	*38*	*51*	2.73	5.08	3.59	*86*	*32*
H_2O	4.88	6.36	4.42	*30*	*-10*	4.83	5.71	4.22	*18*	*-13*	–	–	–	–	–
Total	100	100	100			100	100	100			100	100	100		

[1]difference between the experiment and MELTS; [2]difference between the experiment and HPx-mb16. tr–trace; BKH–Berndt et al. (2005); SD–Sen & Dunn (1994); L–liquid.